

Responses to the comments from Anonymous Referee #1

General comments

Comment G1: *This manuscript reports the implementation and testing of the existing synthetic inflow turbulence generation method (Xie and Castro, 2008) for large-eddy simulations (LES). The LES model in question is the widely used WRF-LES model for small-scale atmospheric problems. The topic is important since the question of how to deal with the missing inflow turbulence information is one of the most important issues in the context of practical applications of LES to small-scale atmospheric problems as well as to other kind of turbulent-flow problems such as e.g. many engineering related problems. The authors correctly point out the particular need for methods to handle the inflow turbulence question in cases when the LES model is nested within a meso-scale atmospheric model domain. The gray zone between the scales resolvable by the meso-scale models and the resolution requirements of LES unavoidably lead to a large gap in the resolution and therefore it becomes very important to somehow incorporate the lacking turbulence information on the inflow boundaries of the LES-domain in some more or less approximative manner.*

The degree of novelty of the present work is not particularly high. This is because the method in question was developed already more than ten years ago, and because the same method has already been implemented in some other LES models such as the PALM model which is also a LES model for small-scale atmospheric problems like WRF-LES. However, in my opinion, this work deserves to be published since it involves a rather systematic study of the properties of the method in the WRF-LES model. Especially, the sensitivity study to the integral length scale provides some new and very likely useful information.

Response: We thank the reviewer for the overall positive comments. To echo the positive feedback from the reviewer, we wish to reiterate that the gray zone issue still remains challenging for sub-kilometre meteorological modelling and there is a great demand for a reliable nesting methodology to enable sub-hundred-metre large-eddy simulations of the atmospheric boundary layer. The WRF model is perhaps the best platform to test such a methodology, whilst PALM has no capability of meso-scale meteorological modelling. As one important step to achieve this target, this study attempts to equip WRF with a well-tested synthetic turbulence inflow scheme (Xie and Castro 2008), which has been implemented and tested on engineering type of codes, such as Star-CD (Xie and Castro, 2009) and OpenFOAM (Kim and Xie, 2016) and the micro-scale meteorology code PALM (PALM, 2017; Maronga et al., 2019). We believe that this new capability will benefit many boundary layer modellers to run a LES for their local areas nested online within a meso-scale domain.

The focus of this paper is to rigorously test and explore the Xie & Castro (2008) method in the meso-to-micro-scale meteorological code WRF, in terms of the sensitivity of integral length scales and the adjustment distance of the mean velocity field, the turbulent Reynolds stresses and the local friction velocity. These are the novelties of the paper.

Comment G2: *A remarkable weakness of the work is that the synthetic-turbulence generation method has not been parallelised. Instead, the root process performs the whole task of the synthetic turbulence generation and then distributes it to those other processes which need this information. As shown in the manuscript (Fig. 1 b), this severely compromises the computational speed even in this kind of rather moderate-sized simulation. In really large simulation set ups with thousands or even tens of thousands of CPU-cores employed, the non-parallelised method becomes totally impractical. Therefore the question about the parallelisation must be discussed more deeply in the manuscript. Note that the problem of parallelising this method has already been solved at least in the PALM-implementation.*

Response: This study is focused on the feasibility of implementing the inflow method (Xie & Castro, 2008) in the meso-to-micro-scale meteorological code WRF and the impact of the key variables (i.e. the integral length scales) on the simulated turbulence development inside the domain. Up to the authors' knowledge, the latter has not been rigorously addressed previously. We appreciate that *the technical parallelisation of the Xie & Castro (2008) method has been done in PALM and that some other researchers (e.g. Kim and Xie, 2016) have also made efforts to technically parallelise the Xie & Castro method. These suggest that technically parallelising this method is not an issue. It is our intention that we test the method inside WRF scientifically and rigorously here and publish our open source code through GMD to allow other WRF-LES users to extend technical capabilities of our code, such as parallelisation.* In response to the reviewer's comment, the following paragraph has been added in Discussion and conclusions:

“This study is focused on the feasibility of implementing the inflow method (Xie & Castro, 2008) in the meso-to-micro-scale meteorological code WRF and the impact of the key variables (i.e. the integral length scales) on the simulated turbulence development inside the domain. This inflow subroutine has previously been implemented in both serial and parallel mode in several codes, including engineering type of codes Star-CD (Xie and Castro, 2009) and OpenFOAM (Kim and Xie, 2016), and the micro-scale meteorology code PALM (PALM, 2017). Although the current implementation in WRF is affordable for a moderate-sized simulation (e.g. tens of meters resolutions), the technical parallelisation of this inflow subroutine in WRF-LES can be the future work for very large simulation domains with high resolutions. Users of our open source subroutine may offer this technical contribution.”

Comment G3: *Generally, the manuscript is quite well structured and written, but some improvements are needed, see the specific comments below. In part of the figures, especially in Fig. 4, the legend texts are too small, please enlarge them.*

Response: The specific comments are responded below. The legend texts in Figs 1, 4, 5, 8 and 9 are enlarged.

Specific comments

Comment: *Page 2, line 4: I find the statement: "The WRF-LES model can capture the intermittency of three-dimensional turbulent eddies." a bit confusing. This should be clarified.*

Response: This sentence is deleted and has been replaced by a statement attached to the previous sentence: “At the microscale, a large eddy simulation (LES) can be activated in the WRF model (WRF-LES), enabling users to simulate the characteristics of energy-containing eddies in the atmospheric boundary layer.”.

Comment: *Page 3, line 16: Just a typo: white noise is typed "while noise".*

Response: This is corrected.

Comment: *Page 3, line 27: Perhaps another reference to PALM could be added here, see*

<https://www.geosci-model-dev-discuss.net/gmd-2019-103/> although this is still currently in the discussion phase.

Response: This additional reference for PALM has been added.

Comment: *Page 6, lines 5 and 6: "...dominant Reynolds stress tensors..." does this possibly mean dominant Reynolds stress components, or something else? Please correct.*

Response: "dominant Reynolds stress tensors" is replaced with "Reynolds stress components".

Comment: *Page 6, lines 14 and 15: "...the vertically same wind direction...". For instance "vertically constant wind direction" would be better wording.*

Response: "the vertically same wind direction" is replaced with "the vertically constant wind direction".

Comment: *Page 7, lines 21 and 22: The last sentence of this paragraph is obvious and could as well be dropped.*

Response: This sentence is removed now.

Comment: *Page 8, lines 8 and 9: " $\langle u'^2 \rangle / u_*'^2$ has a higher value at $z/H = 0.1$ than that at $z/H = 0.5$. This is consistent with the trend that it decreases with height in the boundary layer." I find this, too, kind of obvious and unnecessary to mention.*

Response: This is removed now.

Comment: *Page 8, lines 14-16: "The slower adjustment...can be attributed to a larger shear generated TKE..." I don't really understand the line of thinking here. I think this statement should be better justified and explained.*

Response: This sentence is removed. We have added the following discussion regarding the developing distance for TKE in Section 3.1.3.

"Since the streamwise velocity variance has a major contribution to TKE, the developing distance for TKE is similar to that for the streamwise velocity variance, i.e. about $x/H = 7-8$. The distance needed for different quantities to develop the turbulence differs between each other, and it is about $x/H = 5-15$."

Comment: *Page 8, Sec. 3.1.4: The inflow case profiles of the second moments in Fig. 5 (and also to some extent in Fig. 9) appear wavy compared with the periodic case profiles. I assume that it is very clear for a large majority of the readers that this is because these profiles are not averaged in the stream-wise direction like those of the periodic case. However, I think this should be nevertheless explained in the text.*

Response: We have reprocessed the model output with much smaller time intervals (5 sec now compared with 60 sec previously). The revised profiles in Figs. 5 and 9 are now much smoother.

Comment: *Page 9, lines 16 and 17: The last sentence of this paragraph appears vague. Please, improve it. One reason for my confusion may be that there is no inertial subrange visible in the spectra shown in Fig. 10, probably because of the rather moderate resolution and/or numerically dissipative advection scheme. Moreover, I think that the term "inertial sublayer" is not good. It is better to say inertial subrange because it is not intuitive (or at least I don't find it intuitive) to think about layers in the wave-number space.*

Response: In the previous version, the spectra were calculated based on the spatially distributed data along the cross-stream direction (y) for given (x, z) coordinates. These were averaged for a number of time steps to smooth them. The limit of this approach is that a small number of data along the cross-stream direction (y) were used.

A slightly different approach is adopted in the revised paper. For given (x, y, z) coordinates, a spectrum was calculated based on a time series of 3600 s with an interval of 5 s. Five spectra for ($y/H = 1.76, 2.16, 2.56, 2.96$ and 3.36) at the same (x, z) coordinates were averaged to obtain a smoother one plotted in Fig. 6. The same was used for the new Figure 10. In the text, "inertial sublayer" is replaced by "inertial subrange".

We also added some discussion as,

"It is noted that for a very high resolution, e.g. in the order of magnitude 1 meter, similar as that used in the simulations of PALM (PALM, 2017), the inertial subrange in the spectrum is wider."

Comment: *Page 9, line 32: "...less 1.0...", please, add "than".*

Response: "than" is added.

Comment: *Page 10, line 3: "...the 'accurate' ones...". I assume this refers to that in the case LS1.0 the integral length scales are set as evaluated from the periodic case results, but I am not sure if I understood this correctly. This should be written more clearly.*

Response: "the 'accurate' ones" is replaced with "the 'accurate' (compared with the periodic case) one".

Comment: *Page 10, line 3: I guess LE ratio should be LS ratio.*

Response: "LE ratio equal to one" is replaced with "the LS 1.0 case".

Comment: *Page 10, line 12, "...WRF-LES (v3.6.1) models...". Why models, i.e. why in pluralis form?*

Response: "idealised WRF-LES (v3.6.1) models" is replaced with "an idealised WRF-LES (v3.6.1) model".

Comment: *Page 11, lines 5-7: I find these last two sentences of this paragraph very unclear. If this is to discuss the (so far) lacking parallelisation of the method, it is not sufficient and not at all clear. As stated above in my general comments this issue must be discussed more deeply. It deserves its own paragraph in the Discussion and conclusions section, but should also be better brought up in Sec. 2.3.*

Response: See the response to Comment G2. We have added a paragraph for the discussion about the parallelisation of the method in the third paragraph of the section of Discussion and conclusions

Responses to the comments from Anonymous Referee #2

General comments

Comment G1: *The manuscript “Implementation of a synthetic inflow turbulence generator in idealised WRF v3.6.1 large eddy simulations under neutral atmospheric conditions” by Zhong et al. submitted to the Geoscientific Model Development (GMD) describes the implementation of an existing synesthetic turbulence generator to the Weather Research and Forecasting (WRF) model, with the aim of reducing the inflow fetch distance for nested simulations down to the large-eddy simulation (LES) scale. They tested a neutral boundary layer (NBL) case, and performed sensitivity study of a key length scale in their turbulence generator. The results were then evaluated against a standalone periodic LES simulation.*

This work will benefit the atmospheric community by providing them with a practical engineering tool for improving nested simulations at the LES scale. Implementing a piece of code like this into WRF is no “a walk in the park”, it must have taken the authors a great deal of time and effort. For that I appreciate their efforts, and applaud them for making their code publicly available with this manuscript.

Response: We appreciate the reviewer’s comments on the challenges on implementing an inflow synesthetic turbulence generator in the WRF-LES model. The inflow method was originally developed for engineering applications, and has not been rigorously tested in full-scale atmospheric boundary layer problems. This study extended a well-tested synthetic turbulence inflow scheme (Xie and Castro 2008) into the WRF-LES model. This implementation can be applied to the WRF-LES simulation with a multi-scale seamless nesting case from a meso-scale domain with a km-resolution (where the time-averaged information is known, which can be used as the inputs for the synthetic inflow turbulence generator) down to LES domains with metre resolutions (with additional turbulent information).

Comment G2: *But regarding the contents, I am afraid that I fail to see the scientific novelty with this manuscript. It seems that all they did were to document the performance of an existing method on one particular case. One way to improve this manuscript is for the authors to interpret their results based on more detailed analysis rather than speculation, so that the readers have a more fundamental understanding of the strength and weakness of the synthetic turbulence generator applied to the atmospheric boundary layer flow. For example, regarding Fig. 4f, the authors observed that the TKE profiles at $0.1H$ requires a longer fetch to converge to the periodic solution, and commented that this maybe due to “downward turbulence transport from above”. My suggestion is then don’t stop at this speculation, investigate it by plotting the resolved TKE budgets and prove or disapprove your hypothesis. I have listed a few suggestions in the major comments, but the list is by no means exhaustive.*

Response: We implemented a synthetic turbulence inflow generator (Xie and Castro 2008), which has been implemented and tested on engineering type of codes, such as Star-CD (Xie and Castro, 2009) and OpenFOAM (Kim and Xie, 2016) and the micro-scale meteorology code PALM (PALM, 2017; Maronga et al., 2019), into the WRF-LES model. The focus of this paper is to rigorously test and explore the Xie & Castro (2008) method in a full scale (i.e. very large Re number), in terms of the sensitivity of integral length scales and the adjustment distance of the mean velocity field, the turbulent Reynolds stresses, TKE and the local friction velocity. Our paper will be useful to the users of the Xie & Castro (2008) method implemented in meso-scale models, such as WRF, and the micro-scale meteorology models, such as PALM. Our conclusion in the current paper is that the Xie and Castro (2008) method needs 5-15 boundary layer depths to fully develop the turbulence, and this is consistent with those in Xie & Castro (2008), Kim et al (2013) for engineering scale problems. For a coarser grid resolution of 90 m (vs 20 m in our paper), Munoz-Esparza et al. (2014, 2015) tested both their proposed ‘cell perturbation method’ and the Xie and Castro (2008) method; they concluded that *the cell perturbation*

method needs a fetch of 15-40 boundary layer depths to fully develop the turbulence, while the Xie and Castro (2008) method needs a longer fetch. A significant improvement of this fetch generated by our code is one of the novelties and, together with the study of the impact of the key variables (i.e. the integral length scales) on the simulated turbulence development represents the scientific novelties of the paper.

In response to the reviewer's suggestion to improve the interpretation of the results, we have conducted more detailed analyses (see those responses to each individual comment below, and the revised figures in the paper).

With regards to the comment on discussions of Fig. 4f, we have reprocessed the model output with much smaller time intervals (5 sec now compared with 60 sec previously). The revised profiles in Figs. 5 and 9 are now much smoother. Our statement in the previous version does not stand anymore. Therefore we have removed those sentences. Subsequently, we think it is not necessary to look into the TKE budget. The modified text (in Section 3.1.3) is as below:

“Since the streamwise velocity variance has a major contribution to TKE, the developing distance for TKE is similar to that for the streamwise velocity variance, i.e. about $x/H = 7-8$ ”.

Comment G3: *Finally, please, please improve your English writing, proof read it carefully and invite a native speaker to proofread the manuscript before submission. Overall, I suggest major revisions.*

Response: We checked our English writing, proofed read the revised manuscript carefully, and also invited a native speaker to proofread the manuscript before re-submission.

Major comments

Comment M1: *1. Add more analysis to help interpret your results, as I have mentioned in the overall comments, speculation is hardly helpful. After you document the various mean profiles and turbulence statistics, analyze them to help us understand why.*

Response: We thank the reviewer for this comment. We have re-postprocessed the model output. In particular, we have now used a much big dataset to generate better statistical results and velocity spectra. These have largely helped us to make more solid conclusions rather than speculations.

In response to the reviewer's comment (also please see our reply to General Comment G2), we have conducted the following extra analyses and added interpretations of the results. Correspondingly, the following text (on Paragraph 2 of Section 2.3) has been added or modified in the manuscript:

“The further 1 h outputs with 5 second interval (\sim the advection timescale of the smallest resolved eddies, which is equivalently twice the grid resolution of 20 m) were used for the analysis. In this study, by taking advantage of the homogeneous turbulence in the spanwise direction (Ghannam et al., 2015), we calculate all resolved-scale turbulent quantities by averaging in the spanwise (the y -direction) direction and in time t over the last 1 h period. This averaging is referred to as “the y - t averaging” hereafter, and is denoted by $\langle \varphi \rangle$, for example, for the y - t averaged φ . For a 4D variable, $\varphi(t, x, y, z)$, the y - t averaged φ is a function of x, z , i.e. $\langle \varphi \rangle(x, z)$; for a variable defined on the x - y plane, e.g. friction velocity $u_*(t, x, y)$, the y - t averaging u_* is a function of x , i.e. $\langle u_* \rangle(x)$.”

In this way, a better representation of resolved turbulent statistics is achieved. The various curves in the plots are smoother for clearer interpretations. The spectra cover the information of a wider range of eddy sizes.

We have modified and added the following for the explanation of the new spectrum plots (Section 3.1.5):

“For each x -location, e.g. $x/H = 10$, the spectrum for the inflow case was firstly calculated from the streamwise wind velocity component over a time series of 3600 s with an interval of 5 s for five selected sample locations of y_n ($y/H = 1.76, 2.16, 2.56, 2.96$ and 3.36), namely, $\tilde{u}(t, 2H, y_n, 0.5H)$. The spectral data were then averaged over y_n to give the spectra plotted in Fig. 6. ”

Another new case with mean inflow only containing no inlet velocity perturbations has been conducted. The horizontal slice of instantaneous streamwise velocity component had been added into Fig 2 as a comparison, in order to provide a better understanding of the advantage of this synthetic turbulence generator.

The spatially and temporally averaged vertical profiles of the mean velocity and the Reynolds stresses, and spectrum for $x/H=0$ for the inflow cases have now been added in the corresponding figures. These provide a better understanding of the direct output from the inflow turbulence generator.

More discussion for the interpreting the results are added, see the following responses.

Comment M2: *2. I suggest the authors add a control case where inflow contains no turbulence information, just the mean profiles. This way the readers could have a much better sense of the advantage/power of the turbulence generator by comparing the results to the control case.*

Response: We have run one further case with mean inflow only containing no inlet velocity perturbations. The horizontal slice of instantaneous streamwise velocity components had been added into Fig. 2 as a comparison, in order to provide evidence of the advantage of this synthetic turbulence generator. There is nearly no turbulence generated in the domain even after several hours of simulation (also indicated by the following plot for the vertical profile of TKE - note all of the data, except for the Periodic case, are zero). We have added the following discussions in the revised paper (Paragraph 1 in Section 3.1.1):

“For the inflow case without inlet velocity perturbations, there is nearly no turbulence generated in the domain even after several hours of simulation. This is consistent with other similar tests using engineering CFD codes with no synthetic turbulence added at the inlet, e.g. (Xie and Castro, 2008), which demonstrated that a very long distance (e.g 100 times boundary layer thickness) is needed to allow turbulence to develop. This indicates the importance of imposing synthetic turbulence, or at least some form of random perturbations (e.g. Munoz-Esparza et al., 2015) at the inlet. The inflow case without inlet velocity perturbations is not presented in the later sections. ”

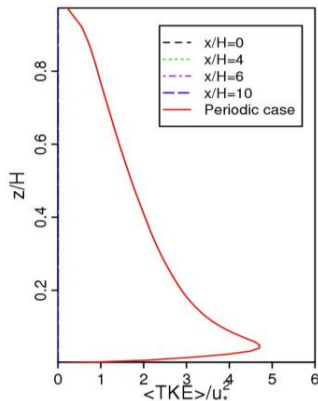


Figure R1: Vertical profile of TKE for the inflow case without inlet velocity perturbations, and for the periodic case.

Comment M3: 3. When presenting the various profiles and spectra, I suggest adding profiles/spectra at $x/H = 0$, i.e., the inlet profiles directly from the turbulence generator. This way, we have a better sense of the direct output from turbulence generator.

Response: The $x/H=0$ profiles for the inflow cases are now added into Figs 5 and 6. The turbulence statistics derived from the current periodic case are used as the input of the inflow turbulence generator. The following are added:

“It is noted that the profiles of the mean velocity and second order moments at the inlet ($x/H = 0$) are overall in a good agreement with these of the periodic case, which further suggests a satisfactory performance of the turbulence generator.” (in Paragraph 1 of Section 3.1.4)

“It is shown that the spectrum at the inlet ($x/H=0$) possesses the most broad range of the $-5/3$ slope compared to the others. There is an evidence of the tendency in the profiles from the inlet downstream to recover to that of the periodic case. The spectrum drops slightly at high wavenumbers from the imposed spectra at $x/H = 0$ to downwind locations, and to recover towards the spectrum of the periodic case. The slight drop suggests a decay of small eddies due to the SGS and molecular viscosities.” (in Paragraph 2 of Section 3.1.5)

Comment M4: 4. I wonder if the shape of the integral length scale profiles in Fig. 1a matter for the results. The step function like integral length scale in the streamwise direction L_x worries me a little bit, and please elaborate on your “canopy” argument for L_x . Furthermore, the relative importance of these integral length scale profiles is also of interest. For example, what if you only vary L_y but keep L_x and L_z the same in your sensitivity tests?

Response: Xie and Castro (2008) and Kim et al (2013) have already reported more sensitivity studies on the effect of integral length scales, including keeping L_x the same and varying L_y and L_z . They found that a 50% variation in L_y and L_z generated a variation less than 4% in the friction velocity, and suggested that for the integral lengths not too far from realistic ones, the turbulent statistics are not very sensitive to the length scales.

Again, we emphasise that the aim here is not to generate a particularly accurate simulation of turbulent atmospheric boundary layer flow. Rather, our intention is to assess the adequacy and potential of the inflow generation technique for the prediction of up to second order moments of turbulent statistics.

It is difficult to analyse mathematically the effect of the step change of integral length scales. However, practically we have not noticed an evident issue. These are consistent with Veloudis et al (2007) and Xie and Castro (2008).

Veloudis, I., Yang, Z., McGuirk, J.J., Page, G.J., Spencer, A.: Novel implementation and assessment of a digital filter based approach for the generation of LES inlet conditions. Flow Turbul. Combust. 79(1), 1–24 (2007)

We have added the modified text on Paragraph 1 of Section 2.3:

“The streamwise length scale (L_x) is specified based on the mean streamwise velocity profile ($\langle u \rangle$) and a constant Lagrangian time scale T (prescribed in Eq. 13), i.e. $L_x = T\langle u \rangle$ using Taylor's hypothesis (turbulence is assumed to be frozen while it is moving downstream with a mean speed of $\langle u \rangle$). The spanwise length scale (L_y) is specified a constant value. The vertical length scale (L_z) is specified a smaller constant value near the bottom and a larger constant value for the upper domain to be closer to the measured length scales, as explained in Xie and Castro (2008) and Veloudis et al. (2007). We conducted a sensitivity study of integral length scales by varying all three baseline L_x , L_y and L_z with a same ratio of 0.6, 0.8, 1.0, 1.2, or 1.4; these individual cases are denoted by “LS0.6”, “LS0.8”, “LS1.0”, “LS1.2”, “LS1.4”, respectively, in which “LS1.0” is the base case.”

Comment M5: 5. *The model setup also worries me. In Page 6, your domain depth is 0.5 km, and if I understand correctly based on your Line 7, the boundary layer depth is also 0.5 km. Such a shallow domain depth might cause undesirable reflections back into your domain, unless you are using radiative top boundary conditions. Is that implemented in WRF? Please comment/give more information on the top boundary condition used.*

Response: For the neutral boundary layer, the results at any altitudes scaled by the boundary layer height could be interpreted for and applied to the cases with other boundary layer heights, e.g. 1000 m.

We have added the following information about the top boundary conditions used in this WRF-LES model, to respond to the reviewer's comment:

“At the top boundary, a rigid lid (`top_lid` in the `namelist.input` file of the WRF-LES model) is specified, and a Rayleigh damping layer of 50 m is used to prevent undesirable reflections (Nottrott et al., 2014; Ma and Liu, 2017) and to maintain a neutral atmospheric boundary layer.”

Minor comments

Comment: 1. *Page 2, Line 4, “The WRF-LES model can capture the intermittency of three dimensional turbulent eddies”. Could you provide a reference please? It would be useful to the readers. I am also curious to learn about studies on turbulence intermittency using WRF-LES.*

Response: This sentence is deleted and has been replaced by a statement attached to the previous sentence: “At the microscale, a large eddy simulation (LES) can be activated in the WRF model (WRF-LES), enabling users to simulate the characteristics of energy-containing eddies in the atmospheric boundary layer.”

Comment: 2. *Page 2, Line 5, “There still remains a challenge for downscaling from mesoscale simulation (down to 1 km) to the LES scale (tens of meters or below) (Doubrawa et al., 2018).” Please, summarize brief what this challenge is.*

Response: More details are added on Paragraph 1 Section 1:

“There still remains a challenge for downscaling from a mesoscale simulation (resolutions down to 1 km, capturing mean information only) to an LES scale (tens of meters or below, capturing additional turbulence information) (Doubrawa et al., 2018; Talbot et al., 2012; Chu et al., 2014; Liu et al., 2011), e.g. the appropriate inflow conditions for an LES domain, and the sub-grid scale turbulence schemes suitable for appropriate treatment of the “gray-zone” resolution domain where neither planetary boundary layer (PBL) nor LES parametrisation schemes apply well.”

Comment: 3. *Page 2, Line 7, “Most WRF-LES models : : : uses: : :” please fix your grammar.*

Response: “uses” is replaced with “use”.

Comment: 4. *Page 2, Line 8, By “These brave assumptions”, you actually meant the one brave assumption of periodic boundary conditions only. Please improve this sentence.*

Response: This sentence is improved as follows:

“However, implicit in the use of periodic boundary conditions is the assumption that atmospheric fields and the underlying landuse have repeated periodic features. This assumption may be unrealistic for real landscapes where landuse patterns - and the atmospheric phenomena coupled to them - can be very heterogeneous.”

Comment: 5. Page 2, Line 12. I am confused about your “As one step moving towards enabling WRF’s capability of nesting: : :”. Why and how would the synthetic turbulence inflow scheme help with nesting? I guess this is related to my earlier point that you need to lay out clearly the difficulties of meso-to-microscale nesting first, before diving into your proposed method.

Response: As mentioned in a response above, there are two key challenges: appropriate sub-scale turbulence schemes and suitable inflow conditions. In this study, we are focusing on the latter, as one step moving forward. Without the synthetic turbulence inflow scheme, it would take a large distance in the LES domain for the simulated turbulent fields to fully develop. The modified text is:

“Here we implement a well-tested synthetic turbulence inflow scheme (Xie and Castro 2008) in the WRF-LES model (v.3.6.1), in which the meso-scale model could provide the mean flow information as the input of the synthetic turbulence inflow scheme. This scheme provides a step towards enabling WRF’s capability of nesting micro-scale turbulent flows within realistic meso-scale meteorological fields.”

Comment: 6. Page 2, Line 18 “turbulence” not “turbulences”.

Response: This is corrected.

Comment: 7. Page 3, Line 21, “It is thus not surprising that a very long distance, e.g. 20–40 boundary layer depths, is normally required to allow a transition to fully developed turbulence.” This statement might be misleading. My understanding is that the cell perturbation method (CPM) of Munoz-Esparza et al. (2014) applied to potential temperature requires only a short distance before turbulence is properly spun up, even for the neutral boundary layer (see their Fig. 7). This is also true when CPM is applied to velocity (Mazzaro et al., 2019, JAMES, 11(7):2311-2329). The author should clarify or give a proper reference to the fetch distance of “20-40 boundary layer depths”.

Response: We thank the reviewer for pointing this out. Figure 7 in Munoz-Esparza et al. (2014) is just a contour plot without any quantitative information. In their later paper using the Cell Perturbation Method (CPM) for neutral boundary layer, Mazzaro et al., 2019 concludes that “while the CPM significantly reduced the effect of these high-TKE regions, with a shorter fetch of 15–20 km” (See their conclusion), which is expected to be consistent with the Fig. 7 in Munoz-Esparza et al. (2014). The neutral boundary layer height used in their papers is 500 m, and a fetch of 15–20 km is equivalent to 30–40 boundary layer depths. Also, in another paper Munoz-Esparza et al. (2015), Fig. 10 shows a quantitative profile of Reynolds-shear stress and the resolved TKE for the development distance, in which a fetch of 15-40 boundary layer depths is mentioned for the turbulence development, while 15 boundary layer depths can achieve values within 10% of the quasi-equilibrium solution for cell perturbation method.

It is to be noted that in Munoz-Esparza et al. (2014, 2015) and (Mazzaro et al., 2019), the inflow forcing is implemented at the west and south boundaries (i.e. both x - and y -directions), while we implemented the inflow turbulence generation at the $x=0$ boundary only. Again, we agree with the authors that the

Cell Perturbation Method (CPM) provides an alternative way of turbulence generation in the modelling of atmospheric boundary layer.

We have added the reference and modified this sentence (on Paragraph 3 of Section 1):

“It is thus not surprising that a large distance of about 20-40 boundary layer depths (Munoz-Esparza et al., 2015; Mazzaro et al., 2019) is normally required to allow a transition to fully developed turbulence.”

Comment: 8. Page 3, Line 25, “flows” not “follows”.

Response: “follows” is replaced with “flows”.

Comment: 9. Page 4, Line 4, “energy-taking resolved eddies” ? This sounds very strange.

Response: “large energy-taking resolved eddies” is replaced with “large energy-containing eddies at the resolved scale”.

Comment: 10. Eqs. 1-2, perhaps you are using the Favre filter in these equations, or perhaps you are using the Boussinesq approximations for the PBL, please clarify. Eqs.1-2 are not the governing equations for compressible flow as you indicated in Line 3.

Response: The WRF-LES solves the fully compressible equations in the flux form which implies an application of the Favre filter, formulated using a terrain-following hydrostatic-pressure vertical coordinate. For an LES domain with flat terrain, the momentum equations can be presented by Equation (2). With an assumption of incompressibility of the atmospheric boundary layer, the continuity equation can be expressed as Equation (1). Being rigorous, we change Equation (1) to the original format by removing the assumption of incompressibility. These are also adopted by other WRF-LES studies (Nottrott et al., 2014; Munoz-Esparza et al., 2015).

Comment: 11. Eq. 7, this is a parameterized TKE equation where turbulent transport and pressure correlation terms are parameterized. It is also written without the buoyancy term, and should therefore only applicable to a vertical depth within the NBL, but not above the boundary layer where stable stratification prevails. Unless the authors intend to adopt an isentropic background state for their simulations, I suggest including the buoyancy terms for completeness. The use of the mixing length “ l ” as the dissipation scale is another assumption that should at least be mentioned.

Response: In response to the comment, we have added the buoyancy term in the equation. Since this study is focused on the inflow turbulence generator using WRF-LES in which the subscale TKE equation is coded based on parameterised terms, we consider it appropriate to present the equation in the parameterised forms.

We have added “dissipation coefficient (for more details about the parameterisation see Moeng et al. (2007)).”

Comment: 12. Eq. 15, please explain the meaning of the “alpha” inside the matrix. It also looks strange that you shall write a_{ij} in a matrix form in Eq. 15. Shouldn't α_{ij} be an element of your matrix, rather the entire matrix itself?

Response: To avoid any misunderstanding, α_{ij} is changed to $[\alpha_{i\beta}]$ to represent the matrix form, while $\alpha_{i\beta}$ in the matrix represents an element of the matrix, following the notations of Equation (18) in Xie and Castro (2008). The calculations of $\alpha_{i\beta}$ follow an iterative order: α_{11} , α_{21} , α_{22} , α_{31} , α_{32} , and α_{33} . This has been added in the manuscript.

Comment: 13. Page 6, Line 9, what do you mean by “a constant Lagrangian time scale T (Eq. 13) using Taylor’s hypothesis”? please give more detail here, how did you determine your “constant T ” value?

Response: This is explained in more details on Paragraph 1 of Section 2.3:

“The streamwise length scale (L_x) is specified based on the mean streamwise velocity profile ($\langle u \rangle$) and a constant Lagrangian time scale T (prescribed in Eq. 13), i.e. $L_x = T\langle u \rangle$ using Taylor’s hypothesis (turbulence is assumed to be frozen while it is moving downstream with a mean speed of $\langle u \rangle$).”

Comment: 14. Page 6, Line 10-11, “canopy height”? Why suddenly canopy height? What’s the purpose of placing a canopy layer in your NBL simulations?

Response: These have been removed as they are not very relevant to this paper. The modified text is:

“The vertical length scale (L_z) is specified a smaller constant value near the bottom and a larger constant value for the upper domain to be closer to the measured length scales, as explained in Xie and Castro (2008) and Veloudis et al. (2007).”

Comment: 15. Page 6, “: : , explained in Xie and Castro (2008)”. Please fix your grammar.

Response: “explained in Xie and Castro (2008)” is replaced with “as explained in Xie and Castro (2008) and Veloudis et al. (2007)”.

Comment: 16. Page 6, Line 14-15, “the vertically same wind direction”, please fix your grammar.

Response: “the vertically same wind direction” is replaced with “the constant wind direction vertically”.

Comment: 17. Page 6, Line 19, “in the lateral direction”, did you mean “spanwise” direction? Same for the rest of this paragraph. Lateral suggests both x - and y -directions.

Response: “in the lateral direction” is replaced with “in the spanwise direction”. This is also corrected in elsewhere of the manuscript.

Comment: 18. Fig. 1, caption, use “relative computation time” as in your main text, rather than “relative computation”.

Response: This is removed.

Comment: 19. Fig. 1, “dashed grey line of 1.0 indicating”, indicates, not indicating.

Response: This is removed.

Comment: 20. Page 7, Line 9, “filtered velocity” rather than “filter velocity”.

Response: “filter velocity” is replaced with “filtered velocity”.

Comment: 21. Page 7, Line 14, and elsewhere. Please double-check on the GMD conventions, but I think you should spell out “Figure” if it is at the beginning of a sentence.

Response: “Fig.” is replaced with “Figure” all over the manuscript now, if it is at the beginning of a sentence.

Comment: 22. Fig. 2. Caption, “(b) The : : :” change to “(b) the : : :”

Response: “The” is replaced with “the”.

Comment: 23. Page 7, Line 16, “are advected and decay downwind: : :”, please fix your grammar.

Response: “are advected and decay downwind: : :” is replaced with “are advected in the domain: : :”.

Comment: 24. Page 7, “can generate realistic well-configured turbulence structures from a short adjustment distance downwind”. The adjustment distance does not look short to me. Judging from your Fig. 2b, it looks like a fetch distance of $x = 5H$ is required at least. Please comment on this.

Response: We have rephrased it to

“This suggests that the synthetic inflow turbulence generator can generate realistic well-configured turbulence structures from an adjustment distance downwind of about $x/H = 5-10$ ”

Comment: 25. Page 7, Line 21 to 22, “and there is no adjustment distance, and instead, an adjustment time to generate fully-developed turbulence structures”. Please fix your grammar.

Response: This sentence is removed now.

Comment: 26. Page 7, Line 28, “plan” or “plane”?

Response: “plan” is replaced with “plane”.

Comment: 27. Fig. 3, I suggest using the “global friction velocity u^* ” from the periodic case to normalize u^* for the inflow case. This way, we could detect the presence of systematic biases in the inflow case, if any.

Response: Now the friction velocity for the inflow case in Fig 3 is scaled by the “global friction velocity” from the periodic case. The relevant modified text is as below:

“The variation of the local friction velocity is within $\pm 0.5\% u_*$ along the streamwise direction for the periodic case and is slightly higher (within $1.5\% u_*$) than that for the inflow case after a downwind distance of $x/H = 7$.”

Comment: 28. Fig. 3. caption “(laterally and temporally)”, laterally and temporally averaged?

Response: “laterally and temporally” is replaced with “the y-t averaged”.

Comment: 29. Page 8, Line 10, “a good agreement against?” Please improve this sentence.

Response: This is modified as follows:

“The horizontal profiles of normalised cross-stream velocity variance ($\langle v'^2 \rangle / u_*^2$) for the inflow case are in a good agreement after a developing distance of $x/H = 10-12$, compared with these for the periodic case.”

Comment: 30. Page 8, Line 12, can you comment on the possible reason for the slow convergence (long fetch distance) of w'^2 at $0.1 z/H$?

Response: This comment was for the figure in the first version. In the current version, as the profiles are smoother, we noticed that the difference is not evident. Therefore, we have revised this in the paper (Paragraph 1 of Section 3.1.3)

“The development of normalised vertical velocity variance ($\langle w'^2 \rangle / u_*^2$) is achieved after a developing distance of about $x/H = 5-10$.”

Comment: 31. Page 8, Line 15, why would “a larger shear-generated TKE” slow down the adjustment at $0.1z/H$? Shouldn't this accelerate the adjustment because more TKE is generated locally independent of the TKE contained in the inflow.

Response: See the above responses, e.g. the reply to Comment 30. This sentence is removed. The modified relevant text is:

“Since the streamwise velocity variance has a major contribution to TKE, the developing distance for TKE is similar to that for the streamwise velocity variance, i.e. about $x/H = 7-8$.”

Comment: 32. Page 8, “downward turbulence transport from above” Did you look at the TKE budget? The transport term of TKE is quite insignificant in the NBL. Unless the inflow case is doing something less. It would be nice if you could present the TKE budgets and compare between the two cases.

Response: See the responses for Comment G2 regarding this comment.

Comment: 33. Page 8, “The red circle dots”, just “red circles” will do.

Response: “The red circle dots” is replaced with “red line”, to be consistent with new plots.

Comment: 34. Page 8, Line 21, “noticed again” or “noted again”?

Response: “noticed again” is replaced with “noted again”.

Comment: 35. Fig. 6, caption “ $\langle u \rangle$ and $\langle u' \rangle$ the laterally averaged mean and streamwise normal Reynolds stress”, how are these Reynolds stresses? These are first-order moments.

Response: $\langle u' \rangle$ is replaced with $\langle u'^2 \rangle$.

Comment: 36. Page 9, Line 17, “is able to sustained”, please fix your grammar.

Response: “is able to sustained” is replaced with “is able to be mostly sustained”.

Comment: 37. Fig. 6, could you include a spectrum at the inlet $x = 0$, so that the readers have an idea of what the synthetic turbulence spectrum looks like?

Response: The spectrum at the inlet $x = 0$ is added and the inertial subrange of $-5/3$ slope is shown in Fig. 6. The relevant modified text is:

“The spectrum drops slightly at high wavenumbers from the imposed spectra at $x/H = 0$ to downwind locations, and to recover towards the spectrum of the periodic case. The slight drop suggests a decay of small eddies due to the SGS and molecular viscosities”

Comment: 38. “A length scale (LS) ratio : : : are tested.” Please fix your grammar.

Response: “A length scale (LS) ratio : : : are tested.” is replaced with “Length scale (LS) ratios : : : are tested.”

Comment: 39. Page 9, bottom line “Fig. 8 (a) shows that $\langle u \rangle / u_*$ is slightly greater for the LS ratio less 1.0 (see Fig. 8a for comparison). This is due to a greater Reynolds shear stress $\langle u'w' \rangle / u_*^2$. I do not understand your explanation. The velocity profile at $z/H = 0.5$ is affected by the divergence of the stresses, rather than the stress itself. How could a large stress value at $z/H = 0.5$ explain the overestimation of the velocity?”

Response: We are sorry that this was confusing. This has been revised to

“Figure 8 (a) shows that $\langle u \rangle / u_*$ is slightly greater for the length scale ratio less than 1.0. This is likely due to a slightly smaller u_* , which is common for smaller integral length scale cases (as shown in Fig. 7).”

Comment: 40. Page 10, Line 1, “Figs. 8(b-d) and (f)” rather than “Fig. 8(b-d)”.

Response: “Fig. 8(b-d) and (f)” is replaced with “Figures 8(b-d) and (f)”.

Comment: 41. Page 10, Line 3, what is the “LE ratio”? did you mean your “LS 1.0” case?

Response: Yes, it is fixed. “LE ratio equal to one” is replaced with “the LS 1.0 case”.

Comment: 42. Page 10, Line 3, why is “LE ratio equal to one” the “accurate ones”? First of all, please fix your grammar. Second, what do you mean by “accurate”?

Response: “the ‘accurate’ ones” is replaced with “the ‘accurate’ (compared with the periodic case) one”. The ‘accurate’ is for the comparison to the periodic case.

Comment: 43. Page 10, Line 5, if all you have to say about Fig. 9 is that it “confirms the findings suggested from Fig. 8”, I would suggest you remove that figure.

Response: More discussion about Figure 9 is added on Paragraph 3 of Section 3.2:

“For $x/H = 10$, both mean and turbulent quantities converge approximately to the periodic case. In general, there are slight differences in $\langle u \rangle / u_*$ between each case. The magnitudes of turbulent quantities for smaller integral length scales are slightly smaller than those for larger integral length scales. This suggests that the mean velocity and the turbulent Reynolds stresses are not very sensitive to the integral length scales if they are not too different from the realistic values.”

Comment: 44. Page 10, Line 9-10, “There is no significant change of the spectra”, depends on what you mean by significant. The differences among these LS cases are similar to those presented in Fig. 6. I would suggest you plot your data on kE - $\log(k)$ plots. First, this avoids the flat 1D spectra issue at the low wavenumbers. Second, it would be much easier to tell the differences if the y-axis is not on a log scale.

Response: Please see our reply to Comment M1. At $x/H=10$, all cases varying integral length scales generally converge to the periodic case with slight changes of the spectrum for small wavenumber turbulence. In the text, “no significant change” has been modified as “slight changes” for the new spectrum. There is no issue of flat spectra at the low wavenumbers for the new plots. In this paper, we present the spectrum plots with the inertial subrange of $-5/3$ slope (indicated in new plots), consistent with those in Xie and Castro (2008). The relevant text is modified (Paragraph 4 of Section 3.2)

“For all cases in the current study, the spectra with various integral length scales generally match those of the periodic case at a developing distance of $x/H = 10$, albeit with slight changes of the spectrum for small wavenumber turbulence. A very small variation of the spectra is within the uncertainty of the calculation of spectrum from the raw data. The spectra show an inertial subrange of $-5/3$ slope, which are consistent as those in the references, such as Xie and Castro (2008).”

“The spectrum in Munoz-Esparza et al. (2015) drops steeper at high wavenumbers, mainly due to a coarser resolution (noticing that their plots were for kE_{u_i} with the inertial subrange of $-2/3$ slope). Our spectrum for E_u has a broad range of the inertial subrange of $-5/3$ slope, indicated in Fig. 6.”

Comment: 45. Page 10, Line 12, “idealised WRF-LES (v3.6.1) models”, model not models

Response: “idealised WRF-LES (v3.6.1) models” is replaced with “an idealised WRF-LES (v3.6.1) model”.

Comment: 46. Page 11, Line 11, “The spectrum of these data shows an inertial subrange”. I strongly recommend you show these in your spectra plots.

Response: The inertial subrange is now shown in the new spectrum plots Figs. 6 and 10.

Comment: 47. Page 11, Line 12, “yields a satisfactory accuracy”. Please, fix your grammar.

Response: We have improved this statement, i.e.

“These tests on WRF also confirm that this method yields a satisfactory accuracy, after having compared *the local friction velocity, the mean velocity, the Reynolds stresses and the turbulence spectra* against the reference data.”

Responses to the comments from Anonymous Referee #3

General Remarks

Comment G1: *The manuscript attempts to address a timely and relevant problem of inflow turbulence generation in large-eddy simulations of realistic atmospheric boundary layer flows. While there is nothing fundamentally wrong with the methodology applied the manuscript has a number of significant deficiencies. The review of previous work in the field is inadequate. The authors make several references to derived work instead of citing the original work (more details are provided under “Specific Remarks”).*

Response: We thank the reviewer for the critical comments, of which many are constructive.

This study attempts to equip WRF-LES with a well-tested synthetic turbulence inflow method (Xie and Castro 2008), which has been implemented and tested on engineering type of codes, such as Star-CD (Xie and Castro, 2009) and OpenFOAM (Kim and Xie, 2016) and the micro-scale meteorology code PALM (PALM, 2017; Maronga et al., 2019). This study can potentially provide a tool to bridge in WRF from mesoscale simulation (down to 1 km resolution) to the micro-scale Large-Eddy Simulations (tens of meters or less resolution) with additional turbulence information at small scales. In particular, we have highlighted the novelties in the revised paper, and have improved the review and citation of previous work in the introduction. More are detailed in the responses to “Specific Remarks”.

Comment G2: *Only neutral boundary layer simulations are carried out and the Coriolis force was not activated. Such setup does not produce a realistic atmospheric boundary layer.*

Response: This study is focused on the feasibility of the inflow generation subroutine on WRF-LES using a periodic run as a control case. It is particularly focused on the sensitivity of the integral length scales on the turbulence development in the full-scale modelling of WRF under neutral atmospheric conditions. Turning off the Coriolis force is to achieve a constant wind direction vertically, enabling an easier interpretation of the impact of the integral length scales on the simulated flows. This kind of configuration (ignoring Coriolis force) has been used in previous work. A WRF-LES study by Ma and Liu (2017) removed the Coriolis force and used pressure gradient as the driving force to achieve a constant wind direction vertically for a simulation over a hill. Testing the Xie and Castro (2008) method for other conditions, such as considering the Coriolis effect, is out of the scope of this paper and can be the future work. Users of our open source subroutine may extend the code for their own applications.

Comment G3: *Furthermore, the synthetic turbulence generation approach of Xie and Castro (2008) was already implemented in WRF by Muñoz-Esparza et al. (2015), so it is not clear what is the original contribution of this work.*

Response: Munoz-Esparza et al. (PoF 2015) focused on their own developed and preferred method - the cell perturbation method, but not on the Xie and Castro (2008) method. To our best knowledge, their code of the Xie and Castro (2008) method has not been contributed as an open source. We made our inflow code (Xie and Castro, 2008) publicly available in this open source journal, i.e. Goescientific Model Development, which is one of the contributions to the community.

In addition, their numeric tests (Muñoz-Esparza et al., 2015) are based on the grid resolution of 90 m. The size of smallest eddy that can be resolved by the LES model is 180 m (i.e. twice the grid resolution). Given a boundary layer height of 500 m in their settings, there are just a small number of eddies resolved (considering the turbulence is anisotropic) in the vertical direction by their model. Our tests here adopt the grid resolution of 20 m. Munoz-Esparza et al. (2015) concluded that *the cell perturbation method*

needs a fetch of 15-40 boundary layer depths to fully develop the turbulence, while the Xie and Castro (2008) method needs more fetch. However, our conclusion in the current paper is that the Xie and Castro (2008) method only needs 5-15 boundary layer depths to fully develop the turbulence, and this is consistent with those in Xie & Castro (2008), Kim et al (2013) for engineering scale problems. This is obviously a new finding derived from a better configured model for the simulations of the full-scale atmospheric boundary layer than that in Muñoz-Esparza et al. (2015), although both use the Xie and Castro (2008) method implemented in WRF-LES.

Xie & Castro (2008) has been implemented in engineering type codes and is successful for wind-tunnel scale (ie. O(1m)) problems, but have not yet been tested rigorously in a meso-scale meteorological model. The focus of our current paper is to rigorously test and explore the Xie & Castro (2008) method in a full scale (i.g. very large Re number) problem, in terms of the sensitivity of integral length scales and the adjustment distance of the mean velocity field, the turbulent Reynolds stresses and the local friction velocity. Our paper will be extremely useful to the users of the Xie & Castro (2008) method in meso-scale meteorological models, such as WRF, and the micro-scale meteorology models, such as PALM. These are the novelties of the paper.

This work bridges the gap, such as in terms of the resolution (we use higher resolution than Munoz-Esparza et al (2014, 2015)), the sensitivity of the turbulent statistics due to the change of integral length scales, for a systematic study of the properties of the method in the WRF-LES model. Of course, we are not able to address everything in this aspect. We also do agree with the authors that Munoz-Esparza et al (2014, 2015)) provide an alternative for turbulence generation for such applications.

Comment G4: *Finally, some of the conclusions about the effectiveness of the synthetic turbulence generation approach are not supported by the results presented in the manuscript. In particular, the length of the fetch needed to achieve the equilibrium boundary layer is underestimated.*

Response: In response to the reviewer's comment, we have conducted more detailed analyses, including re-postprocessing more model output (i.e. using the higher-frequency output - every 5 sec in contrast to every 1 min in the previous analysis) to generate better turbulence statistics and spectra (see the Figs. 5, 6, 9, and 10, for example). These have largely helped us to make more solid conclusions on the effectiveness of the synthetic turbulence generation approach. See more specific replies to the specific remarks.

The length of the fetch needed to achieve the equilibrium boundary layer has been carefully assessed for the turbulent Reynolds stresses, TKE and the local friction velocity. Our conclusion in the current paper is that the Xie and Castro (2008) method needs 5-15 boundary layer depths to fully develop the turbulence, and this is consistent with those in Xie & Castro (2008), Kim et al (2013) for engineering scale problems. For a coarser grid resolution of 90 m (vs 20 m in our paper), Munoz-Esparza et al. (2015) concluded that "the cell perturbation method needs a fetch of 15-40 boundary layer depths to fully develop the turbulence, while the Xie and Castro (2008) method needs more fetch". We speculate it is mainly because Munoz-Esparza et al. (2015) used a much coarser mesh in their tests.

We have added/modified the following related text:

"Since the streamwise velocity variance has a major contribution to TKE, the developing distance for TKE is similar to that for the streamwise velocity variance, i.e. about $x/H = 7-8$. The distance needed for different quantities to reach a converged state differs from each other, and it is about $x/H = 5-15$."

Comment G5: *Taking all the above into account I do not recommend the manuscript for publication in the journal Geoscientific Model Development.*

Response: Anyway, we have taken the reviewer's critical (including many constructive) points. We would like to cite here some points from the other two reviewers:

"this work deserves to be published since it involves a rather systematic study of the properties of the method in the WRF-LES model. Especially, the sensitivity study to the integral length scale provides some new and very likely useful information."

"The gray zone between the scales resolvable by the meso-scale models and the resolution requirements of LES unavoidably lead to a large gap in the resolution and therefore it becomes very important to somehow incorporate the lacking turbulence information on the inflow boundaries of the LES-domain in some more or less approximative manner."

"This work will benefit the atmospheric community by providing them with a practical engineering tool for improving nested simulations at the LES scale. Implementing a piece of code like this into WRF is no "a walk in the park", it must have taken the authors a great deal of time and effort. For that I appreciate their efforts, and applaud them for making their code publicly available with this manuscript."

We have carefully addressed the major concerns raised by the reviewer, and also improved the manuscript by addressing the specific remarks suggested by the reviewer as below.

Specific Remarks

Comment: *Page 2, line 2 – The reference to Nottrott et al. is not appropriate, since Nottrott et al. did not develop WRF. Proper reference would be Skamarock and Klemp (JCP 2008).*

Response: We thank the reviewer for the suggestion. This reference Skamarock and Klemp (JCP 2008) was cited when the WRF model was mentioned in our previous version (i.e. in the sentence before Page 2, line 2). Here, the reference to Nottrott et al. is now replaced with "(Skamarock and Klemp, 2008)".

Comment: *Page 2, line 7 – Doubrawa et al. 2018 is certainly not the first or most important reference related to WRF-LES.*

Response: Doubrawa et al. 2018 is a study on the downscaling from mesoscale simulation to the LES, i.e. linked to the terra incognita range of grid resolutions. More related references are added in the revised paper, i.e. "Doubrawa et al., 2018; Talbot et al., 2012; Chu et al., 2014; Liu et al., 2011".

Comment: *Page 2, line 11 – This is not an example of a fundamental study. Nunalee et al. (2014) reported on LES using WRF model based on a tracer dispersion field study and compared simulation results to field study observations.*

Response: We thank the reviewer for the comment. In response to the comment, we've added the first study of testing nested LES in WRF by Moeng et al. (2007) and other relevant studies in the revised paper. The word of "fundamental" is removed and more details about studies (with some references) are added as follows,

“Therefore such periodic WRF-LES simulations are restricted to *studies* of the atmospheric boundary layer flow with a single domain (e.g. Zhu et al., 2016; Kirkil et al., 2012; Kang and Lenschow, 2014; Ma and Liu, 2017) or the outermost domain for the nested cases (e.g. Moeng et al., 2007; Khani and Porte-Agel, 2017; Nunalee et al., 2014).”

Nunalee et al. (2014) used periodic conditions for the parent domain in the nested WRF-LES simulations for the tracer dispersion study and also compared meteorological conditions (i.e. hourly mean vertical profiles of wind speed, potential temperature and wind direction in their Fig. 4) with the field measurements. Nunalee et al. (2014) is kept in the revised paper as an example case for the use of periodic conditions for the parent domain in nested WRF-LES cases.

Comment: Page 2, line 14 – *Munoz-Esparza et al. (PoF 2015) have already implemented synthetic turbulence inflow scheme by Xie and Castro (2008), so it is not clear what is the original contribution of this work.*

Response: This is also commented in Comment G3. See our responses to Comment G3.

Comment: Page 2, line 20 – *A space is missing between year and semicolon, here, and on numerous places throughout the manuscript.*

Response: This is due to the formatting of Endnote for multiple citations. A space is added between multiple citations and this has been checked throughout the manuscript.

Comment: Page 2, line 26 – *However, the velocity profile could be modified, also it can vary in time.*

Response: These is for the discussion of the library-based method and recycling-rescaling based method, which are normally applicable to the idealised LES simulations of stationary and equilibrium flows. We have added the following here,

“The turbulence profile determined by the geometry of the precursor simulation can be added on the top of any given mean profile, which could be modified and varied in time for more realistic applications.”

Comment: Page 3, line 16 – *More recent reference that expands and improves on Muñoz-Esparza et al. (2015) is Muñoz-Esparza and Kosovic (2018).*

Response: The more recent reference is added as follows:

“Munoz-Esparza and Kosovic (2018) extended the cell perturbation method of the inflow turbulence generation to non-neutral atmospheric boundary layers.”

Comment: Page 4, line 4 – *A subgrid scale scheme does not parameterize small unresolved eddies, instead it parameterizes the effect of small unresolved eddies on the resolved field.*

Response: This is modified as follows: “which computes large energy-containing eddies at the resolved scale directly and parameterises the effect of small unresolved eddies on the resolved field using subgrid-scale (SGS) turbulence schemes (Moeng et al., 2007).”

Comment: *Page 5, Equation 9, 12, etc. – The notation using plus sign is confusing since subscript m indicates the velocity component.*

Response: We are sorry that the reviewer was confused here because we used ‘ m ’ to index two different quantities by mistake. We have now corrected it. In the revised manuscript, we’ve added “ m , the index that the averaging operator is applied, denotes the m -th element of a vector (one-dimensional data series of, for example, the digital-filtered velocity, u , in (9) below), k is the number of elements for the two-point distance of $k\Delta x$ ” for explanation when these first appear in Eq. (8). In addition, “ m ” in Eqs. (12) and (13) is replaced by “ β ” to indicate velocity components. “ j ” in Eqs. (14) and (15) is also replaced by “ β ”. These notations follow those adopted by Xie & Castro (2008).

Comment: *Page 6, line 15 – Why is Coriolis turned off if simulation of flow in an atmospheric boundary layer is the goal?*

Response: This is also commented in Comment G2. See the responses to Comment G2.

Comment: *Page 7, line 6 – Doubling the computational time is a significant increase that needs to be justified.*

Response: This is due to that “the additional computational time associated with subroutine of the synthetic inflow turbulence generator and data passing, which is not parallelised, while the main code WRF is parallelised”.

We emphasize again that this study is focused on the feasibility of implementing the inflow method (Xie & Castro, 2008) in the meso-to-micro-scale meteorological code of WRF and the impact of the key variables (i.e. the integral length scales) on the simulated turbulence development inside the domain. Up to the authors’ knowledge, the latter has not been rigorously addressed previously. We appreciate that *the technical parallelisation of the Xie & Castro (2008) method has been done in PALM and some other researchers (e.g. Kim and Xie, 2016) have also made efforts to technically parallelise the Xie & Castro method. These suggest that technically parallelising this method is not an issue. It is our intention that we test the method inside WRF scientifically and rigorously here and publish our open source subroutine through GMD to allow other WRF-LES users to extend technical capabilities of our code, such as parallelisation.* A paragraph in the Discussion and conclusions section is added for the discussion about the parallelisation of the method, i.e.

“This study is focused on the feasibility of implementing the inflow method (Xie & Castro, 2008) in the meso-to-micro-scale meteorological code WRF and the impact of the key variables (i.e. the integral length scales) on the simulated turbulence development inside the domain. This inflow subroutine has previously been implemented in both serial and parallel mode in several codes, including engineering type of codes Star-CD (Xie and Castro, 2009) and OpenFOAM (Kim and Xie, 2016), and the micro-scale meteorology code PALM (PALM, 2017). Although the current implementation in WRF is affordable for a moderate-sized simulation (e.g. tens of meters resolutions), the technical parallelisation of this inflow subroutine in WRF-LES can be the future work for very large simulation domains with high resolutions. Users of our open source subroutine may offer this technical contribution.”

Comment: Page 7, line 7 – *The adjustment distance should be more precisely quantified.*

Response: “about $x/H = 5-10$ ” is added in the revised paper.

Comment: Page 8, line 2 – *Instead of symbols, the stresses should be defined as: "horizontal profiles of normal and shear turbulent stresses normalized by surface friction velocity."*

Response: Symbols have been removed. The following text is added, i.e.

“horizontal profiles of normalised mean streamwise velocity component, normal and shear turbulent stresses, and TKE”.

Comment: Page 8, line 7 – *Normalized streamwise variance matches well at $x/H = 7$ or 8 and not at $x/H = 5$.*

Response: “ $x/H = 5$ ” is replaced with “ $x/H = 7-8$ ”.

Comment: Page 8, line 10 – *Below $z/H = 0.3$ the profile of cross-stream variance differs significantly for any x/H .*

Response: It has been modified as follows:

“The horizontal profiles of normalised cross-stream velocity variance ($\langle v'^2 \rangle / u_*^2$) for the inflow case are in a good agreement after a developing distance of $x/H = 10-12$, compared with those for the periodic case.”

Comment: Page 8, line 12 – *The development is not achieved at all, since only at the end of the domain the values of $\langle w'^2 \rangle / u_*^2$ obtained using the synthetic turbulence generation method are the same as those from the simulation involving periodic domain. Also, what is shown in the figures is the fetch, not the time scale.*

Response: This comment was for the figure in the first version. In the current version, as the profiles are smoother, we noticed that the difference is not evident. Therefore, we have revised this in the paper.

“The development of normalised vertical velocity variance ($\langle w'^2 \rangle / u_*^2$) is achieved after a developing distance of about $x/H = 5-10$.”

The time scale has been changed to “length scale”.

Comment: Page 8, line 13 – *Figures show that the fetch needed for different quantities to reach the equilibrium values differs significantly between them. For example, vertical velocity variance does not reach equilibrium. Since it is a component of TKE, TKE also requires a long fetch to reach the equilibrium.*

Response: See our reply to the Comment G4. We have regenerated and re-examined these plots carefully. Based on these smoother profiles, we are able to reach more solid conclusions. These plots suggest that the *fetch needed for different quantities to reach the equilibrium values differs only slightly between them, considering a small uncertainties (errors) due to the limited averaging time.*

The fetch needed for different quantities is also discussed in the responses to Comment G4.

Comment: *Page 8, line 18 – Same as above, these should be labeled as normal and shear turbulent stresses normalized by surface friction velocity.*

Response: Symbols have been removed. The following text is added, i.e.

“normalised mean streamwise velocity component, normal and shear turbulent stresses, and TKE”.

Comment: *Page 8, line 22 – A sentence should not begin with a symbol.*

Response: “The normalised mean streamwise velocity component” is added before the symbol.

Comment: *Page 8, line 23 – In “matches closely to that: : ;,” “to” should be omitted.*

Response: “to” is removed.

Comment: *Page 8, line 24 – Same as above, instead of symbols names of the terms should be used.*

Response: This is modified as “The normalised streamwise velocity variance”.

Comment: *Page 9, line 9 - The spectral roll-off depends on the numerics not on the turbulence generation scheme, so this is questionable conclusion. Also, flat spectra over a decade of wave numbers is not realistic. Furthermore, there is not apparent inertial range (-5/3) slope in the results presented in Figure 6.*

Response: In the previous version, we conducted spectral analysis using the spatial data along the cross-stream direction (y) with given values of x ($x/H=2, 4, 6$ and 10) and z ($=0.5H$) and then averaged the spectrum over time to generate the results in Figure 6 in the original manuscript. Now a different method is adopted: for given values of x and z , we conduct spectral analysis using the time series of 3600 s with an interval of 5 s for five selected sample locations of y_n ($y/H = 1.76, 2.16, 2.56, 2.96$ and 3.36), namely, $\tilde{u}(t, 2H, y_n, 0.5H)$, and then an average over y_n yields the data plotted in Fig. 6 in the revised manuscript. This method is in essence used to analyse experimental time series data from point measurement; when applied to the LES data, it yields a fairly good inertial subrange as shown in the new Figure 6, as well as in new Figure 10.

We have modified and added the following (in Section 3.1.5):

“For each x -location, e.g. $x/H = 10$, the spectrum for the inflow case was firstly calculated from the streamwise wind velocity component over a time series of 3600 s with an interval of 5 s for five selected sample locations of y_n ($y/H = 1.76, 2.16, 2.56, 2.96$ and 3.36), namely, $\tilde{u}(t, 2H, y_n, 0.5H)$. The spectral data were then averaged over y_n to give the spectra plotted in Fig. 6.”

“The spectrum drops slightly at high wavenumbers from the imposed spectra at $x/H = 0$ to downwind locations, and to recover towards the spectrum of the periodic case. The slight drop suggests a decay of small eddies due to the SGS and molecular viscosities”

“The spectrum in Munoz-Esparza et al. (2015) drops steeper at high wavenumbers, mainly due to a coarser resolution (noticing that their plots were for kE_{u_i} with the inertial subrange of -2/3 slope). Our spectrum for E_u has a broad range of the inertial subrange of -5/3 slope, indicated in Fig. 6.”

Comment: *Page 9, line 14 – If current work does not differ from Munoz-Esparza et al. (2015), what is new in the present manuscript?*

Response: This is also raised in Comment G3. See the responses to Comment G3.

Comment: *Page 9, line 24 – Instead of “slightly affects,” it should be “affects slightly.”*

Response: As suggested, this is now corrected.

Comment: *Page 9, line 30 – As before, words should be used instead of symbols.*

Response: Symbols have been removed. The following text is added, i.e.

“normalised mean streamwise velocity component, normal and shear turbulent stresses, and TKE”.

Comment: *Page 10, line 3 – It is not clear what is meant by “ ‘accurate’ ones...”*

Response: “the ‘accurate’ ones” is replaced with “the ‘accurate’ (compared with the periodic case) one”. The ‘accurate’ is for the comparison to the periodic case.

Comment: *Page 10, line 16 – It is not clear what is the purpose of the statement starting with “It is not trivial: : :” This statement by itself is of little relevance, the question is: What is the relevance?*

Response: This has been modified:

“It is not trivial to estimate the integral length scales as the primary input of the inflow turbulence generator.” is replaced with “It is important to estimate the integral length scales, which are the key inputs of the inflow turbulence generator.”

Comment: *Page 10, line 21 – The adjustment fetch should be quantified. It is not short.*

Response: This is now quantified, i.e. “after a short adjustment distance” is replaced with “after an adjustment distance of $x/H=5-15$ ”.

Comment: *Page 11, line 12 – The statement related to “: : :a satisfactory accuracy” is an imprecise qualitative statement. It should be stated what is the accuracy satisfactory in comparison to.*

Response: We have improved this statement, i.e.

“These tests on WRF also confirm that this method yields a satisfactory accuracy, after having compared *the local friction velocity, the mean velocity, the Reynolds stresses and the turbulence spectra* against the reference data.”

Implementation of a synthetic inflow turbulence generator in idealised WRF v3.6.1 large eddy simulations under neutral atmospheric conditions

Jian Zhong¹, Xiaoming Cai^{1*} and Zheng-Tong Xie²

5 ¹School of Geography, Earth & Environmental Sciences, University of Birmingham, Edgbaston, Birmingham, B15 2TT, UK

²School of Engineering Sciences, University of Southampton, Southampton, SO17 1BJ, UK

Correspondence to: Xiaoming Cai (x.cai@bham.ac.uk)

10 **Abstract:** A synthetic inflow turbulence generator was implemented in the idealised Weather Research and Forecasting large eddy simulation (WRF-LES v3.6.1) model under neutral atmospheric conditions. This method is based on an exponential correlation function, and generates a series of two-dimensional slices of data which are correlated both in space and in time. These data satisfy a spectrum with a near ‘-5/3’ inertial subrange, suggesting its excellent capability for high Reynolds number atmospheric flows. It is more computationally efficient than other synthetic turbulence generation approaches, such as three-
15 dimensional digital filter methods. A WRF-LES simulation with periodic boundary conditions was conducted to provide *a priori* mean profiles of first- and second-moments of turbulence for the synthetic turbulence generation method and the results of the periodic case were also used to evaluate the inflow case. The inflow case generated similar turbulence structures to those of the periodic case after a short adjustment distance. The inflow case yielded a mean velocity profile and second-moment profiles that agreed well with those generated using periodic boundary conditions, after a short adjustment distance. For the
20 range of the integral length scales we tested, the impact of the inflow case on the mean velocity profiles is negligible, whereas its influence on the second-moment profiles is evident, in particular for very small integral length scales. This implementation enables a WRF-LES simulation of a horizontally inhomogeneous case with non-repeated surface landuse patterns and can be extended so as to conduct a multi-scale seamless nesting simulation from a meso-scale domain with a km-resolution down to LES domains with metre resolutions.

25

Key words: Inflow turbulence generator, Large eddy simulation, Exponential correlation function, Atmospheric boundary layer.

1 Introduction

30 Atmospheric boundary layer flow involves a wide range of scales of eddies, from quasi two-dimensional structures at the mesoscale scales to three-dimensional turbulence (normally with higher Reynolds number, i.e. $Re \sim 10^8$ - 10^9) at the microscale (Munoz-Esparza et al., 2015). The Weather Research and Forecasting (WRF) model (Skamarock and Klemp, 2008) provides the capability of simulating atmospheric systems at a variety of scales. At the mesoscale and synoptic scales, the WRF model

allows grid nesting for downscaling from 10-100 km to 1-10 km using a fully compressible and non-hydrostatic Reynolds-averaged Navier-Stokes (RANS) solver (Skamarock and Klemp, 2008), which captures the behaviours of mean flows only. At the microscale, a large eddy simulation (LES) can be activated in the WRF model (WRF-LES), enabling users to simulate the characteristics of energy-containing eddies in the atmospheric boundary layer. There still remains a challenge for downscaling from a mesoscale simulation (resolutions down to 1 km, capturing mean information only) to an LES scale (tens of meters or below, capturing additional turbulence information) (Doubrawa et al., 2018; Talbot et al., 2012; Chu et al., 2014; Liu et al., 2011), e.g. the appropriate inflow conditions for an LES domain, and the sub-grid scale turbulence schemes suitable for appropriate treatment of the “gray-zone” resolution domain where neither planetary boundary layer (PBL) nor LES parametrisation schemes apply well. Consequently, these two scales of problems are studied separately. Most LES models of atmospheric boundary layer flow at the microscale use periodic boundary conditions and simplified large-scale geostrophic forcing for idealised simulations. However, implicit in the use of periodic boundary conditions is the assumption that atmospheric fields and the underlying landuse have repeated periodic features. This assumption may be unrealistic for real landscapes where landuse patterns - and the atmospheric phenomena coupled to them - can be very heterogeneous. Therefore such periodic WRF-LES simulations are restricted to studies of the atmospheric boundary layer flow with a single domain (e.g. Zhu et al., 2016; Kirkil et al., 2012; Kang and Lenschow, 2014; Ma and Liu, 2017) or the outmost domain for the nested cases (e.g. Moeng et al., 2007; Khani and Porte-Agel, 2017; Nunalee et al., 2014). Here we implement a well-tested synthetic turbulence inflow scheme (Xie and Castro 2008) in the WRF-LES model (v.3.6.1), in which the meso-scale model could provide the mean flow information as the input of the synthetic turbulence inflow scheme. This scheme provides a step towards enabling WRF’s capability of nesting micro-scale turbulent flows within realistic meso-scale meteorological fields.

Dhamankar et al. (2018) reviewed three broad classes of methods to generate the turbulent inflow conditions for LES models, mainly for engineering applications. The first class is the library-based method, which relies on an external turbulence library to provide inflow turbulence. The turbulence library can be based on either: (a) the precursor/concurrent simulation (e.g. Munters et al., 2016) on the same geometry to a main LES simulation; or (b) a pre-existing database (e.g. Schluter et al., 2004; Keating et al., 2004) from experiments or computations (on a different geometry to a main LES simulation). Although this method is usually limited to specialised applications, it can provide good-quality inflow turbulence. The second class is the recycling-rescaling based method (e.g. Lund et al., 1998; Morgan et al., 2011), in which the velocity field is recycled from a downstream boundary back to the upstream inlet. Although this method may be effective in producing well-established turbulence, there are some limitations, e.g. the requirements of an equilibrium region near the inlet and a relatively large domain. The turbulence profile determined by the geometry of the precursor simulation can be added on the top of any given mean profile, which could be modified and varied in time for more realistic applications. The third class is the synthetic turbulence generator, which includes a variety of methods such as the Fourier transform-based method (e.g. Kraichnan, 1970; Lee et al., 1992), proper orthogonal-decomposition-based method (e.g. Berkooz et al., 1993; Kerschen et al., 2005), digital-filter-based method (e.g. Xie and Castro, 2008; Klein et al., 2003; Kim et al., 2013), diffusion-based method (e.g. Kempf et

al., 2005), vortex method (e.g. Benhamadouche et al., 2006) and synthetic eddy method (e.g. Jarrin et al., 2006). The synthetic turbulence generator has the potential to be used for a wide range of flows. Due to the imperfection of the synthetic turbulence, which is not directly derived from generic flow equations, these methods normally require some inputs and a certain adjustment distance for turbulence to be well-established. For more information about the above synthetic turbulence generation methods, readers are recommended to read Tabor and Baba-Ahmadi (2010), Wu (2017) and Bercin et al. (2018).

Several other methods have been developed to generate inflow turbulence for atmospheric boundary layer flow in nested WRF-LES models. Mirocha et al. (2014) introduced simple sinusoidal perturbations to the potential temperature and horizontal momentum equations near the inflow boundaries. This method can speed up the development of turbulence and generally has a satisfactory performance in the nested WRF-LES domains, providing promising results. Munoz-Esparza et al. (2014) extended the perturbation method of Mirocha et al. (2014) and proposed four methods, i.e. point perturbation method, cell perturbation method, spectral inertial subrange method and spectral production range perturbations, to generate perturbations of potential temperature for a buffer region near the nested inflow planes. The cell perturbation method was found to have the best performance regarding the adjustment distance for the turbulence to be fully-developed. It has the advantages of negligible computational cost, minimal parameter tuning, not requiring *a priori* turbulent information, and efficiency to accelerate the development of turbulence. Munoz-Esparza et al. (2015) further generalised the cell perturbation method of Munoz-Esparza et al. (2014) under a variety of large-scale forcing conditions for the neutral atmospheric boundary layer. The perturbation Eckert number (describing the interaction between the large-scale forcing and the buoyancy contribution due to the perturbation of potential temperature) was identified as the key parameter that governs the transition to turbulent flow for nested domains. They found an optimal Eckert number to establish a developed turbulent state under neutral atmospheric conditions. Generally speaking, these methods impose “white-noise” perturbations, thus having a flat spectrum, to a variable (e.g. temperature) at the inlet, and the model dynamics will “process” the signals once these signals are advected into the domain, e.g. to dissipate high-wavenumber signals quickly and to adjust low-wavenumber signals gradually. These methods are not the classic inflow turbulence generation methods, which are aimed at providing spatially and temporally correlated wind fields with appropriate power spectra. It is thus not surprising that a large distance of about 20-40 boundary-layer depths (Munoz-Esparza et al., 2015; Mazzaro et al., 2019) is normally required to allow a transition to fully-developed turbulence. The optimisation and generalisation of these methods would also require intensive testing. Munoz-Esparza et al. (2014) commented that ‘the use of temperature perturbations presents an alternative’. Munoz-Esparza and Kosovic (2018) extended the cell perturbation method of the inflow turbulence generation to non-neutral atmospheric boundary layers.

Due to its accuracy, efficiency and, in particular, the capability for high Reynolds number flows, the synthetic inflow turbulence generator (Xie and Castro, 2008) has been implemented and tested on codes developed for engineering applications, such as Star-CD (Xie and Castro, 2009) and OpenFOAM (Kim and Xie, 2016), and the micro-scale meteorology code PALM (PALM, 2017; Maronga et al., 2019). This study focuses on an implementation of this synthetic inflow turbulence generator

(Xie and Castro, 2008) in the idealised WRF-LES (v3.6.1) model under neutral atmospheric conditions. In this paper, Section 2 describes the methodology of WRF-LES model and the technique of the synthetic inflow turbulence generator; Section 3 presents the results of the WRF-LES model with the use of the synthetic inflow turbulence generator; and Section 4 states the conclusions and future work.

5 2 Methodology

2.1 WRF-LES model

The atmospheric boundary layer is simulated by the compressible non-hydrostatic WRF-LES model, which computes large energy-containing eddies at the resolved scale directly and parameterises the effect of small unresolved eddies on the resolved field using subgrid-scale (SGS) turbulence schemes (Moeng et al., 2007). The Favre-filtered equations are (Nottrott et al., 2014; Munoz-Esparza et al., 2015):

$$\frac{\partial \tilde{p}}{\partial t} + \frac{\partial \tilde{p} \tilde{u}_j}{\partial x_j} = 0 \quad (1)$$

$$\frac{\partial \tilde{u}_i}{\partial t} + \frac{\partial \tilde{u}_i \tilde{u}_j}{\partial x_j} = \nu \frac{\partial^2 \tilde{u}_i}{\partial x_j \partial x_j} - \frac{1}{\tilde{\rho}} \frac{\partial \tilde{p}}{\partial x_i} - \frac{\partial \tau_{ij}}{\partial x_j} + \tilde{F}_i, \quad (2)$$

where i (or j) = 1, 2, 3, represents the component of the spatial coordinate, \tilde{u}_i is the filtered velocity, x_i is the spatial coordinate, t is the time, \tilde{p} denotes the filtered pressure, $\tilde{\rho}$ is the filtered density, ν is the fluid kinematic viscosity, τ_{ij} are the SGS stresses, \tilde{F}_i represents external force terms (normally involving the Coriolis force caused by the rotation of the Earth and the large-scale geostrophic forcing).

For the closure of Eq. (2), τ_{ij} are parameterised using a SGS model. In this study, the 1.5-order turbulent kinetic energy (TKE) SGS model is used,

$$\tau_{ij} = -2\nu_{sgs} \tilde{S}_{ij}, \quad (3)$$

where \tilde{S}_{ij} is the filtered strain-rate tensor and calculated as,

$$\tilde{S}_{ij} = \frac{1}{2} \left(\frac{\partial \tilde{u}_i}{\partial x_j} + \frac{\partial \tilde{u}_j}{\partial x_i} \right), \quad (4)$$

ν_{sgs} denotes the SGS eddy-viscosity and is defined as,

$$\nu_{sgs} = C_k \ell k_{sgs}^{1/2}, \quad (5)$$

where C_k is a model constant, ℓ is the SGS length scale and under neutral conditions, ℓ equals the grid volume of size (Δ) (Deardorff, 1970),

$$\Delta = (\Delta x \Delta y \Delta z)^{1/3}, \quad (6)$$

k_{sgs} is the SGS TKE with the transport equation

$$5 \quad \frac{\partial k_{sgs}}{\partial t} + \frac{\partial}{\partial x_i} (k_{sgs} \tilde{u}_i) = -\frac{v_{sgs}}{Pr} \frac{g}{\theta_0} \frac{\partial \tilde{\theta}}{\partial z} + 2v_{sgs} \tilde{S}_{ij} \tilde{S}_{ij} + (v + v_{sgs}) \frac{\partial^2 k_{sgs}}{\partial x_i \partial x_i} - C_\varepsilon \frac{k_{sgs}^{1.5}}{\ell}, \quad (7)$$

where $\tilde{\theta}$ is the filtered potential temperature, Pr is the turbulent Prandtl number, C_ε is dissipation coefficient (for more details about the parameterisation see Moeng et al. (2007)). Without loss of generality, the “ $\tilde{\cdot}$ ” notation for all filtered variables is omitted hereafter.

2.2 Synthetic inflow turbulence generator

10 The synthetic inflow turbulence generator in Xie and Castro (2008) adopted the digital filter-based method and is used in this study. For simplicity, a one-dimensional problem (the streamwise velocity, u , along the x -direction) is used as an illustration to describe this method. The two-point velocity correlations $R_{uu}(k\Delta x)$ are assumed to be represented by an exponential function:

$$\frac{\overline{u_m u_{m+k}}}{\overline{u_m u_m}} = R_{uu}(k\Delta x) = \exp\left(-\frac{\pi|k|}{2n}\right), \quad (8)$$

15 where m , the index that the averaging operator is applied, denotes the m -th element of a vector (one-dimensional data series of, for example, the digital-filtered velocity, u , in (9) below), k is the number of elements for the two-point distance of $k\Delta x$, n is related to the integral length scale $L = n\Delta x$ with the grid size of Δx , u_m is the digital-filtered velocity,

$$u_m = \sum_{k=-N}^N b_j r_{m+k}, \quad (9)$$

where r_m is a sequence of random data with mean $\overline{r_m} = 0$ and variance $\overline{r_m r_m} = 1$, N is related to the length scale for the filter (here $N \geq 2n$), and b_j is the filter coefficient and can be estimated from

$$b_k = \tilde{b}_k / (\sum_{j=-N}^N \tilde{b}_j^2)^{1/2}, \text{ where } \tilde{b}_k \cong \exp\left(-\frac{\pi|k|}{n}\right). \quad (10)$$

For a two-dimensional filter coefficient, it can be obtained that

$$b_{jk} = b_j b_k, \quad (11)$$

which will then be used to filter the two-dimensional random data at each time step,

$$25 \quad \varphi_\beta(t, x_j, x_k) = \sum_{j=-N_j}^{N_j} \sum_{k=-N_k}^{N_k} b_{jk} r_{m+j, m+k}, \quad (12)$$

where β indicates the velocity component. At the next time step, the filtered velocity field is calculated as,

$$\Psi_{\beta}(t + \Delta t, x_j, x_k) = \Psi_{\beta}(t, x_j, x_k) \exp\left(-\frac{\pi\Delta t}{2T}\right) + \varphi_{\beta}(t, x_j, x_k) \left[1 - \exp\left(-\frac{\pi\Delta t}{T}\right)\right]^{0.5}, \quad (13)$$

where T is the Lagrangian time scale representing the persistence of the turbulence, $\varphi_{\beta}(t, x_j, x_k)$ is calculated based on Eq. (12). Xie and Castro (2008) demonstrated that Eq. (13) satisfies the correlation functions in an exponential form in space and in time. The two-dimensional filter in Xie and Castro (2008) is more computationally efficient than a three-dimensional filter.

5 Finally, the velocity field is obtained by using the simplified transformation proposed by Lund et al. (1998),

$$\tilde{u}_i = \bar{u}_i + \alpha_{i\beta} \Psi_{\beta}, \quad (14)$$

where

$$[\alpha_{i\beta}] = \begin{bmatrix} (\tilde{R}_{11})^{1/2} & 0 & 0 \\ \tilde{R}_{21}/\alpha_{11} & (\tilde{R}_{22} - (\alpha_{21})^2)^{1/2} & 0 \\ \tilde{R}_{31}/\alpha_{11} & (\tilde{R}_{32} - \alpha_{21}\alpha_{31})/\alpha_{22} & (\tilde{R}_{33} - (\alpha_{31})^2 - (\alpha_{32})^2)^{1/2} \end{bmatrix}, \quad (15)$$

and $\tilde{R}_{i\beta}$ is the resolved Reynolds stress tensor, which can be estimated based on measurements or other simulations with

10 periodic boundary conditions. The calculations of $\alpha_{i\beta}$ follow an iterative order: α_{11} , α_{21} , α_{22} , α_{31} , α_{32} , and α_{33} .

2.3 Model coupling and configuration

In this study, we firstly configured a WRF-LES model with periodic boundary conditions in both streamwise and spanwise directions to obtain *a priori* mean profiles of first- and second-moments of turbulence, such as the vertical profiles of mean velocity and Reynolds stress components, which are required as input by the synthetic inflow turbulence generator. Additional essential quantities as input of the inflow generator are three integral length scales in the x , y and z directions, denoted by L_x , L_y and L_z , respectively (or L_i , $i=x,y,z$). For the inflow BASE case (denoted by LS1.0), the vertical profiles of L_i are specified as functions of z/H , where H is the boundary layer height (500 m in this study), shown as Fig. 1, similar to those in Xie and Castro (2008). The streamwise length scale (L_x) is specified based on the mean streamwise velocity profile ($\langle u \rangle$) and a constant Lagrangian time scale T (prescribed in Eq. 13), i.e. $L_x = T\langle u \rangle$ using Taylor's hypothesis (turbulence is assumed to be frozen while it is moving downstream with a mean speed of $\langle u \rangle$). The spanwise length scale (L_y) is specified as a constant value. The vertical length scale (L_z) is specified as a smaller constant value near the bottom and a larger constant value for the upper domain to be closer to the measured length scales, as explained in Xie and Castro (2008) and Veloudis et al. (2007). We conducted a sensitivity study of integral length scales by varying all three baseline L_x , L_y and L_z with a same ratio of 0.6, 0.8, 1.0, 1.2, or 1.4; these individual cases are denoted by "LS0.6", "LS0.8", "LS1.0", "LS1.2", "LS1.4", respectively, in which "LS1.0" is the base case. The size of the computational domain is 9.98 km \times 2.54 km \times 0.5 km (in x , y and z directions), with the resolutions of $\Delta x = \Delta y = 20$ m and stretched Δz (from about 3 m up to 27 m). The grid number is then 499 \times 127 \times 49. In order to achieve the constant wind direction vertically, the Coriolis force is not activated in this study. The external driving force is specified as a constant pressure gradient force in Eq. (2), similar to that used in Ma and Liu (2017), resulting in a prevailing wind speed of about 10 m s $^{-1}$ at the domain top. At the top boundary, a rigid lid ("top_lid" in the "namelist.input" file of the

WRF-LES model) is specified, and a Rayleigh damping layer of 50 m is used to prevent undesirable reflections (Nottrott et al., 2014; Ma and Liu, 2017) and to maintain a neutral atmospheric boundary layer.

For the cases with the synthetic turbulence at the inlet and periodic conditions in the spanwise direction, the constant pressure gradient force is not necessary anymore. Instead, a pressure-drop between the inlet and outlet is implicitly derived from the prescribed mean momentum profiles as part of the synthetic inflow and the outflow boundary conditions in the solver. The periodic case is used for the validation of the results from the inflow case. The WRF-LES is solved at a time step of 0.2 s. A spin-up period of 6 h is adopted for all inflow cases to allow turbulence inside the domain to reach quasi-equilibrium. The further 1 h outputs with 5 second interval (~ the advection timescale of the smallest resolved eddies, which is equivalently twice the grid resolution of 20 m) were used for the analysis. In this study, by taking advantage of the homogeneous turbulence in the spanwise direction (Ghannam et al., 2015), we calculate all resolved-scale turbulent quantities by averaging in the spanwise (the y -direction) direction and in time t over the last 1 h period. This averaging is referred to as “the y - t averaging” hereafter, and is denoted by $\langle \varphi \rangle$, for example, for the y - t averaged φ . For a 4D variable, $\varphi(t, x, y, z)$, the y - t averaged φ is a function of x, z , i.e. $\langle \varphi \rangle(x, z)$; for a variable defined on the x - y plane, e.g. friction velocity $u_*(t, x, y)$, the y - t averaging u_* is a function of x , i.e. $\langle u_* \rangle(x)$.

In the synthetic inflow turbulence generator, a uniform mesh is used with resolutions of $\Delta y = 20$ m (same as that on the physical inlet of the WRF-LES domain) and $\Delta z = 4.2$ m (slightly larger than the smallest vertical grid spacing of the WRF-LES domain). The three filtered velocity components at the inlet from the inflow generator are then interpolated onto the vertically non-uniform mesh in the WRF-LES domain. It should be noted that the grid resolution can differ between the inflow patch and the inlet of the WRF-LES domain. The standalone synthetic turbulence generator code in Xie and Castro (2008) was originally run on a single processor, whereas the WRF-LES simulation is run in parallel mode. It is therefore necessary to ensure that each processor in the parallel mode has the same information of the 2-dimensional slice of flow field before each processor can extract the corresponding patch from the same 2-dimensional inlet data. In this implementation, the synthetic turbulence generator code is firstly run on the master processor at each WRF-LES time step. The generated inlet data are then passed to other processors. The flow field at the inlet of each corresponding processor was then be updated at every time step accordingly. The additional computational time for the inflow case is associated with the synthetic inflow turbulence generator and data passing, i.e. non-parallelisation of the current inflow generator. Increasing the integral length scale would increase the computation time since bigger arrays are constructed and computed for the filtered velocity in the synthetic inflow turbulence generator, as in Eq. (9) for the larger integral length scale.

3 Results

3.1 BASE case output

3.1.1 Horizontal slices of instantaneous streamwise velocity component

Figure 2 illustrates the horizontal slices of instantaneous streamwise velocity component at $z/H = 0.1$ in the periodic case, the synthetic inflow case (LS1.0 in Fig. 1a), and the inflow case without inlet perturbations (with mean information only) after 6 hours' simulation time. The synthetic turbulence structures imposed at the inlet are advected in the domain, and are adjusted by the model dynamics at further downwind distances. After an adjustment distance (about $x/H = 5-10$), the inflow case (LS1.0) clearly generates turbulence streaks, which are similar to these in the periodic case. Other quantities that may further demonstrate this adjustment distance will be discussed in the following subsections. This suggests that the synthetic inflow turbulence generator can generate realistic well-configured turbulence structures from an adjustment distance downwind of about $x/H = 5-10$. For the inflow case without inlet velocity perturbations, there is nearly no turbulence generated in the domain even after several hours of simulation. This is consistent with other similar tests using engineering CFD codes with no synthetic turbulence added at the inlet, e.g. (Xie and Castro, 2008), which demonstrated that a very long distance (e.g. 100 times boundary layer thickness) is needed to allow turbulence to develop. This indicates the importance of imposing synthetic turbulence, or at least some form of random perturbations (e.g. Munoz-Esparza et al., 2015) at the inlet. The inflow case without inlet velocity perturbations is not presented in the later sections.

3.1.2 Development of local friction velocity

Figure 3 shows the development of the $y-t$ averaged local friction velocity, $\langle u_* \rangle(x)$, for the periodic case and the inflow BASE case (LS1.0), normalised by u_* , the $x-y-t$ -averaged friction velocity for the periodic case. The variation of the local friction velocity is within $\pm 0.5\%$ u_* along the streamwise direction for the periodic case and is slightly higher (within 1.5% u_*) than that for the inflow case after a downwind distance of $x/H = 7$. There is a larger variation close to the inlet region ($x/H < 7$) for the inflow case. This is because the imposed turbulence on the inflow plane is 'synthetic', which develops in a certain distance in the WRF-LES domain.

3.1.3 Horizontal profiles of mean flow and turbulence quantities

Figure 4 illustrates the $y-t$ averaged horizontal profiles of normalised mean streamwise velocity component, normal and shear turbulent stresses, and TKE at $z/H = 0.1$ and $z/H = 0.5$ for the periodic case and the inflow case (LS1.0), respectively. These horizontal profiles show the development of synthetic turbulence generated by the inflow generator. There are only slight differences in normalised mean streamwise velocity component ($\langle u \rangle / u_*$) between the periodic case and the inflow case. This suggests that the inflow case reproduces successfully the desired mean wind profile. The curves of normalised streamwise velocity variance ($\langle u'^2 \rangle / u_*^2$) for both cases match well with each other from $x/H = 7-8$, although there is a sudden jump close

to the inlet and a subsequent decrease until the location of convergence. The horizontal profiles of normalised cross-stream velocity variance ($\langle v'^2 \rangle / u_*^2$) for the inflow case are in a good agreement after a developing distance of $x/H = 10-12$, compared with those for the periodic case. The development of normalised vertical velocity variance ($\langle w'^2 \rangle / u_*^2$) is achieved after a developing distance of about $x/H = 5-10$. The length scale of the development of shear turbulent stress ($\langle u'w' \rangle / u_*^2$) is about $x/H = 5 - 15$. Since the streamwise velocity variance has a major contribution to TKE, the developing distance for TKE is similar to that for the streamwise velocity variance, i.e. about $x/H = 7-8$. The distance needed for different quantities to reach a converged state differs from each other, and it is about $x/H = 5-15$.

3.1.4 Vertical profiles of mean flow and turbulence quantities

Figure 5 shows the $y-t$ averaged vertical profiles of the normalised mean streamwise velocity component, normal and shear turbulent stresses, and TKE at a series of downwind locations, $x/H = 0, 4, 6$ and 10 , for the inflow case (LS1.0). Inflow cases are not averaged in the streamwise direction so that the development of turbulence at each downwind location (x/H) can be investigated. Red lines in Fig. 5 are the spatially (including both in the streamwise and spanwise directions) and temporally averaged vertical profiles for the periodic case. It is noted again that these data for the periodic case are also used as the inputs for *a priori* turbulence information required by the synthetic inflow turbulence generator. The normalised mean streamwise velocity component ($\langle u \rangle / u_*$) profiles of the inflow case match closely those of the periodic case. Although the sampled data are limited, this suggests that the inflow case achieves the desired the mean wind profile.. It is noted that the profiles of the mean velocity and second order moments at the inlet ($x/H = 0$) are overall in a good agreement with these of the periodic case, which further suggests a satisfactory performance of the turbulence generator. The normalised streamwise velocity variance ($\langle u'^2 \rangle / u_*^2$) converges towards the periodic profile after $x/H = 6$ as shown in Fig. 5 (b). Although the vertical profiles of $\langle v'^2 \rangle / u_*^2$, $\langle w'^2 \rangle / u_*^2$ and $\langle TKE \rangle / u_*^2$ for the inflow case show small variations between different locations, they are all in a good agreement with the data of the periodic case. These are consistent with the results shown in Fig. 4. The Reynolds shear stress $\langle u'w' \rangle$, which is the cross correlation between the streamwise and vertical velocity fluctuations, usually converges slower than the normal Reynolds stresses, e.g. $\langle v'^2 \rangle$. Overall, the synthetic inflow turbulence generator performs well in terms of the development of the mean flow and the turbulence quantities against the data from the periodic case.

3.1.5 Spectral analysis

Figure 6 illustrates the spectra of the streamwise wind component at a series of downwind locations ($x/H = 0, 4, 6$, and 10) at $z/H = 0.5$ for the periodic case and the inflow case (LS1.0). For each x -location, e.g. $x/H = 10$, the spectrum for the inflow case was first calculated from the streamwise wind velocity component over a time series of 3600 s with an interval of 5 s for five selected sample locations of y_n ($y/H = 1.76, 2.16, 2.56, 2.96$ and 3.36), namely, $\tilde{u}(t, 2H, y_n, 0.5H)$. The spectral data were then averaged over y_n to give the spectra plotted in Fig. 6.

The spectrum for the periodic case is calculated using the same method as that used for the inflow case, with an additional average over the streamwise direction x . It is shown that the spectrum at the inlet ($x/H=0$) possesses the most broad range of the $-5/3$ slope compared to the others. There is an evidence of the tendency in the profiles from the inlet downstream to recover to that of the periodic case. The spectrum drops slightly at high wavenumbers from the imposed spectra at $x/H = 0$ to downwind locations, and to recover towards the spectrum of the periodic case. The slight drop suggests a decay of small eddies due to the SGS and molecular viscosities. The spectrum in Munoz-Esparza et al. (2015) drops steeper at high wavenumbers, mainly due to a coarser resolution (noticing that their plots were for kE_{u_i} with the inertial subrange of $-2/3$ slope). Our spectrum for E_u has a broad range of the inertial subrange of $-5/3$ slope, indicated in Fig. 6. This is partially attributed to the fact that our resolution of 20 m in the horizontal direction is much finer than their resolution of 90 m. In other words, the size of the smallest eddy (twice the grid resolution) that can be resolved by the LES model is 40 m in our paper vs 180 m in Munoz-Esparza et al. (2015). Munoz-Esparza et al. (2015) also compared the stochastic perturbation method with those obtained using Xie and Castro (2008). These confirm that synthetic turbulence with an inertial subrange in the spectrum generated by using Xie and Castro (2008) method is able to be mostly sustained in WRF-LES for a high resolution. It is noted that for a very high resolution, e.g. in the order of magnitude 1 meter, similar as that used in the simulations of PALM (PALM, 2017), the inertial subrange in the spectrum is wider.

3.2 Sensitivity tests of integral length scale in the flow cases

It is not trivial to optimise the integral length scales of the inlet turbulence generator. Therefore, it is necessary to conduct sensitivity tests of the integral length scales. Figure 7 shows the influence of integral length scale on the development of local friction velocity. Length scale ratios from 0.6 to 1.4 to those (L_x, L_y and L_z) in the LS1.0 case are tested. For all inflow cases, there is a sudden change near the inlet due to the imposed inflow turbulence. The adjustment distance to well-established turbulence is generally shorter for the case with the smaller integral length scale, i.e. about $x/H = 2-7$ for the cases LS0.6-1.4. This suggests that the imposed integral length scales for the inflow turbulence affect slightly the convergence to well-developed turbulence. It is also observed that a variation of $\pm 40\%$ in the integral length scales in the cases LS0.6-1.4 yields a variation of less than 3% in the local friction velocity after about $x/H = 5$. This suggests that the sensitivity of the tested integral length scales on the local friction velocity is not significant in the WRF-LES model, which is consistent with that in engineering type CFD solvers in Xie and Castro (2008). Once the inflow turbulence is established (e.g. after $x/H = 10$), the local friction velocity is slightly greater for larger integral length scales.

Figure 8 shows the effects of integral length scale on the horizontal profiles of the normalised mean streamwise velocity component, normal and shear turbulent stresses, and TKE at $z/H = 0.5$. Figure 8 (a) shows that $\langle u \rangle / u_*$ is slightly greater for the length scale ratio less than 1.0. This is likely due to a slightly smaller u_* , which is common for smaller integral length scale cases (as shown in Fig. 7). Figures 8 (b-d) and (f) show that in general the normal stresses, $\langle u'^2 \rangle / u_*^2$, $\langle v'^2 \rangle / u_*^2$, $\langle w'^2 \rangle / u_*^2$, and

$\langle TKE \rangle / u_*^2$ increase as the length scale ratio increases. This is because small eddies tend to decay faster than large eddies. It is crucial to note that for those with the integral length scales close to the ‘accurate’ (compared with the periodic case) one, i.e. the LS 1.0 case, the development distance to converged turbulence is shorter compared to other cases.

5 Figure 9 shows effects of integral length scale at a typical streamwise location ($x/H = 10$) on vertical profiles of the mean velocity, normal and shear turbulent stresses and TKE. These profiles support the conclusions drawn from Fig. 8. For $x/H = 10$, both mean and turbulent quantities converge approximately to the periodic case. In general, there are slight differences in $\langle u \rangle / u_*$ between each case. The magnitudes of turbulent quantities for smaller integral length scales are generally smaller than those for larger integral length scales. This suggests that the mean velocity and the turbulent Reynolds stresses are not very
10 sensitive to the integral length scales if they are not too different from the realistic values.

Figure 10 shows the effect of the integral length scale on the spectra of the streamwise velocity component at $x/H = 10$ and $z/H = 0.5$. For all cases in the current study, the spectra with various integral length scales generally match those of the periodic case at a developing distance of $x/H = 10$, albeit with slight changes of the spectrum for small wavenumber
15 turbulence. A very small variation of the spectra is within the uncertainty of the calculation of spectrum from the raw data. The spectra show an inertial subrange of -5/3 slope, which are consistent as those in the references, such as Xie and Castro (2008).

4 Discussion and conclusions

A synthetic inflow turbulence generator (Xie and Castro, 2008) was implemented in an idealised WRF-LES (v3.6.1) model
20 under neutral atmospheric conditions. A WRF-LES model with periodic boundary conditions was firstly configured to provide *a priori* turbulence statistical data for the synthetic inflow turbulence generator. The integral length scales were estimated at appropriate ratios to the boundary layer height as in (Xie and Castro, 2008). The results from the inflow cases were then compared with those from the periodic case. It is important to estimate the integral length scales, which are the key inputs of the inflow turbulence generator. Therefore sensitivity tests were conducted for the response of the local friction velocity, the
25 mean flow, the Reynolds stresses, and the turbulence spectra for the flow cases for varying integral length scales.

The inflow case with the baseline integral length scales generates similar turbulence structures to those for the periodic case after an adjustment distance of $x/H = 5-15$. The WRF-LES model with the inflow generator reproduces realistic features of turbulence in the neutral atmospheric boundary layer. The development of local friction velocity suggests that a downwind
30 distance of about $x/H = 7$ is required to recover the local friction force for the inflow case, which is consistent with in the findings of Xie and Castro (2008) and Kim et al (2013). Keating et al. (2004) suggested a development distance of about 20 half-channel depth for modelling a plane channel flow. The difference between this value and our results may be owe to the

different synthetic turbulence generation approaches Keating et al. (2004) adopted. Laraufie et al. (2011) suggested that an increase in the Reynolds number decreases the adjustment distance when a synthetic inflow turbulence generator is used. For our case of the atmospheric boundary layer here, the Reynolds number is extremely large. Thus adopting synthetic inflow turbulence generator for the atmospheric boundary layer should also be advantageous in engineering applications. Regarding the minimum resolution required to generate turbulence synthetically, our presented results confirm that the tested grid resolution sufficiently resolves the important features.

Horizontal and vertical profiles of mean velocity and second-moment statistics further confirm that a short adjustment distance is required for the development of synthetic turbulence. The mean velocity profiles at all tested locations in the domain were close to the desired profiles, while the turbulence second moment statistics profiles were in reasonable agreement with the desired profiles about $x/H = 5-15$ downwind of the inlet. The adjustment distances of second moments are crucial for the assessment of the synthetic inflow turbulence generator. Reducing the integral length scales can shorten the adjustment distance. We found varying the integral length scale does not materially influence the mean velocity profiles, but affects the turbulence second moment statistics more noticeably. The synthetic inflow turbulence generator requires additional computational time compared to periodic boundary conditions. This will be certainly improved by running the synthetic inflow generation subroutine in parallel as a future task. This study is focused on the feasibility of implementing the inflow method (Xie & Castro, 2008) in the meso-to-micro-scale meteorological code WRF and the impact of the key variables (i.e. the integral length scales) on the simulated turbulence development inside the domain. This inflow subroutine has previously been implemented in both serial and parallel mode in several codes, including engineering type of codes Star-CD (Xie and Castro, 2009) and OpenFOAM (Kim and Xie, 2016), and the micro-scale meteorology code PALM (PALM, 2017). Although the current implementation in WRF is affordable for a moderate-sized simulation (e.g. tens of meters resolutions), the technical parallelisation of this inflow subroutine in WRF-LES can be the future work for very large simulation domains with high resolutions. Users of our open source subroutine may offer this technical contribution.

In summary, the synthetic inflow turbulence generator is implemented successfully into the idealised WRF-LES model. The generated two-dimensional slices of data are correlated both in space and in time in the exponential form. The spectrum of these data shows a broad inertial subrange of $-5/3$ slope, and this again suggests the capability of the method to generate high Reynolds number flows. These tests on WRF also confirm that this method yields a satisfactory accuracy, after having compared the local friction velocity, the mean velocity, the Reynolds stresses and the turbulence spectra against the reference data. The WRF-LES model with the synthetic turbulence generator provides promising results as evaluated against the periodic case. The limitation of this method is the requirement of *a priori* turbulence statistic data and integral length scales, which can be estimated by the similarity theory of the atmospheric boundary layer or experimental data. Sensitivity studies have been performed to address this issue, in particular in terms of effect of the integral length scale. We conclude that within a certain range of the integral length scale, the numerical results are not significantly sensitive. The implementation of the

synthetic inflow turbulence generator (Xie and Castro, 2008) can be extended to the WRF-LES simulation of a horizontally inhomogeneous case with non-repeated surface land-use **patterns**, and be further developed for the multi-scale seamless nesting case from a meso-scale domain with a km-resolution down to LES domains with metre resolutions.

5 *Code and data availability.*

The standard version of WRF v3.6.1 is available at http://www2.mmm.ucar.edu/wrf/users/download/get_sources.html. The coupling WRF v3.6.1 code with the synthetic inflow turbulence generator and case settings are archived on Zenodo (<https://doi.org/10.5281/zenodo.3668352>).

10 *Author contributions.*

The study was conceived by XC and ZX; JZ implemented the synthetic inflow turbulence generator code (from ZX) to the WRF-LES model (v3.6.1) and ran model simulations; all authors contributed to writing the manuscript.

Competing interests.

15 The authors declare that they have no conflict of interest.

Acknowledgements.

This work is part of the CityFlocks project, sponsored by the UK Natural Environment Research Council (NERC: NE/N003195/1). This work used the ARCHER UK National Supercomputing Service (<http://www.archer.ac.uk>).

20

25

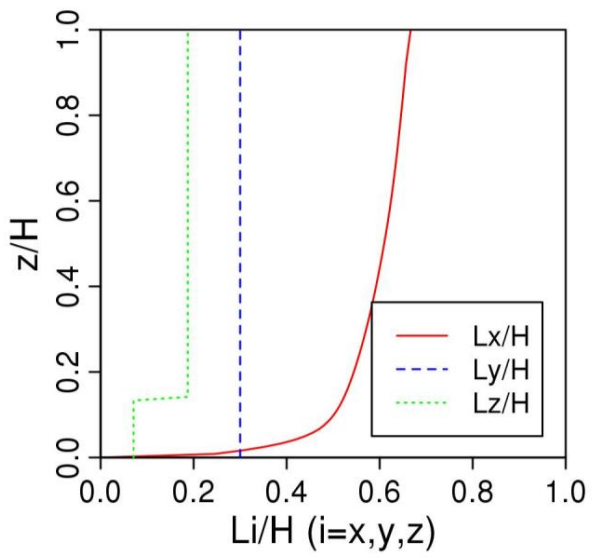


Figure 1: Integral length scales prescribed at the inlet used in the inflow BASE case (LS1.0).

5

10

15

20

25

30

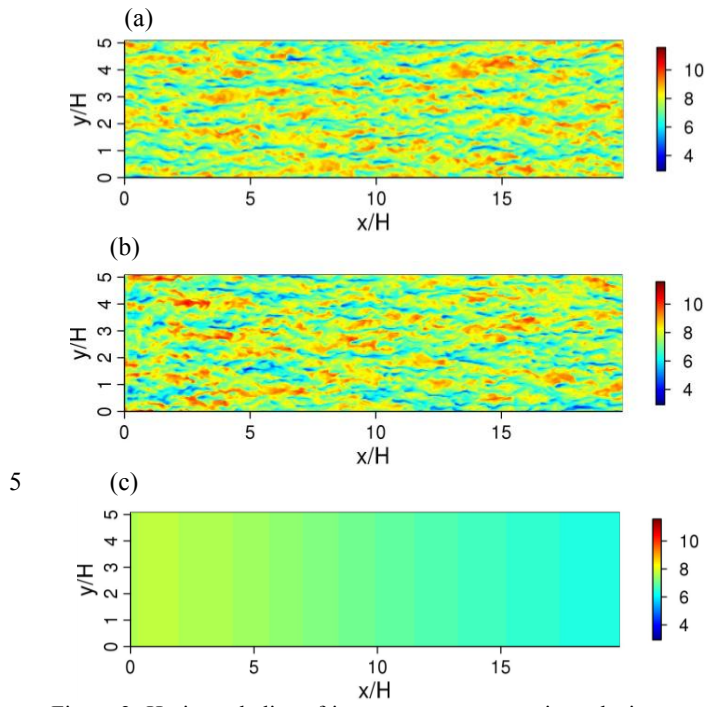


Figure 2: Horizontal slice of instantaneous streamwise velocity component, u (m s^{-1}), at $z/H=0.1$ after 6 hours' simulation: (a) the fully periodic case, (b) the synthetic inflow BASE case (LS1.0), and (c) the inflow case without perturbations at the inlet.

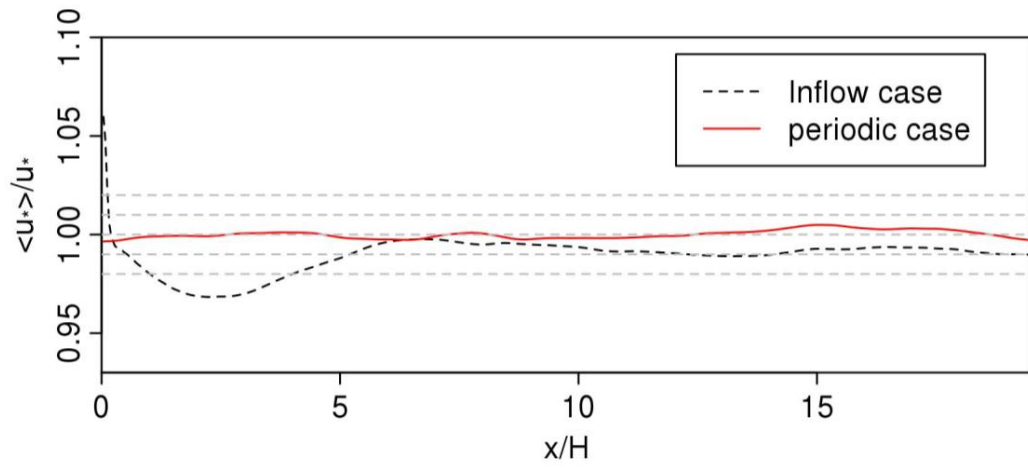


Figure 3: Spatial variation of $\langle u_* \rangle / u_*$ for the periodic case and the inflow case (LS1.0), where $\langle u_* \rangle$ is the y - t averaged local friction velocity and u_* is the x - y - t -averaged friction velocity for the periodic case.

5

10

15

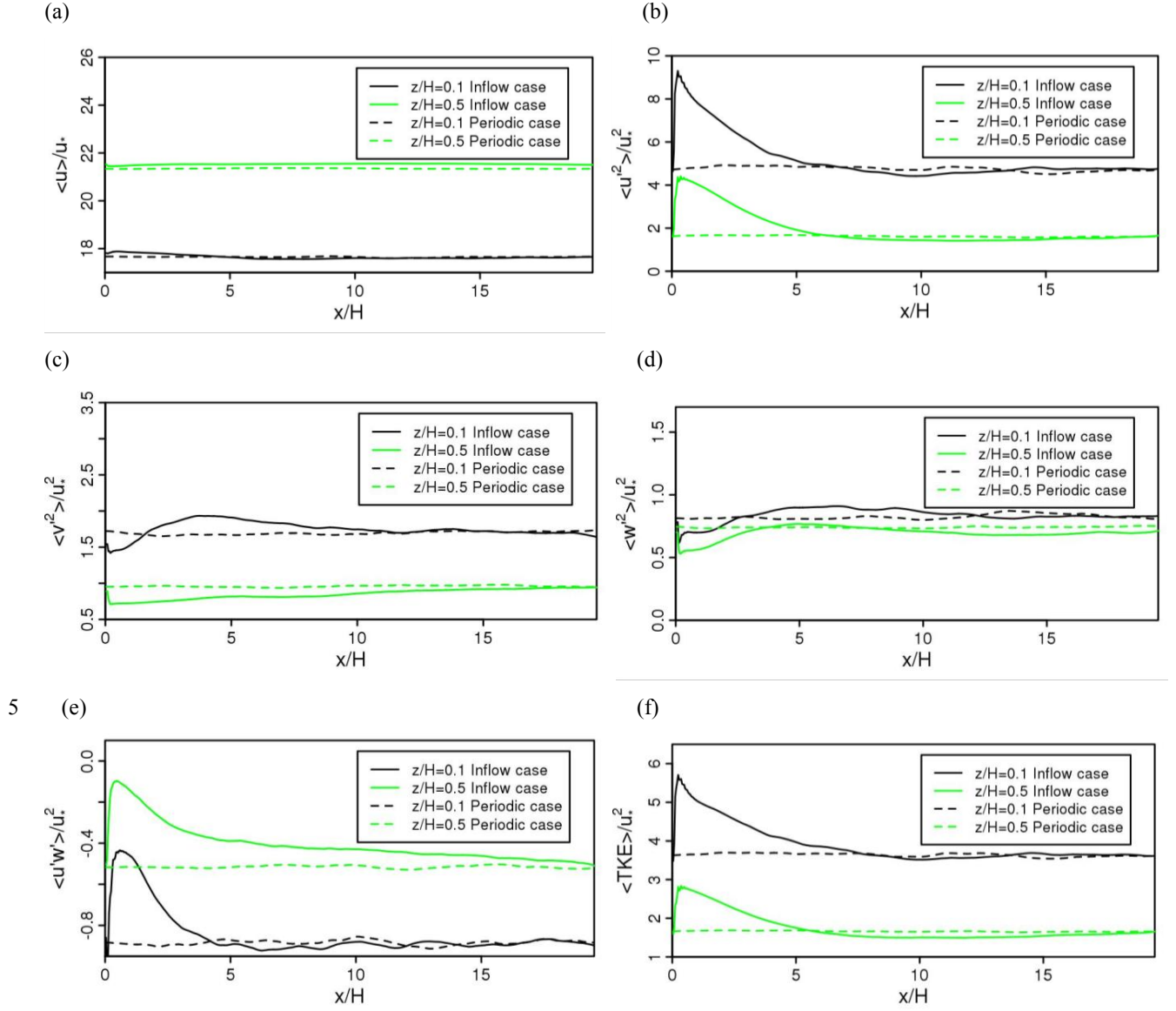
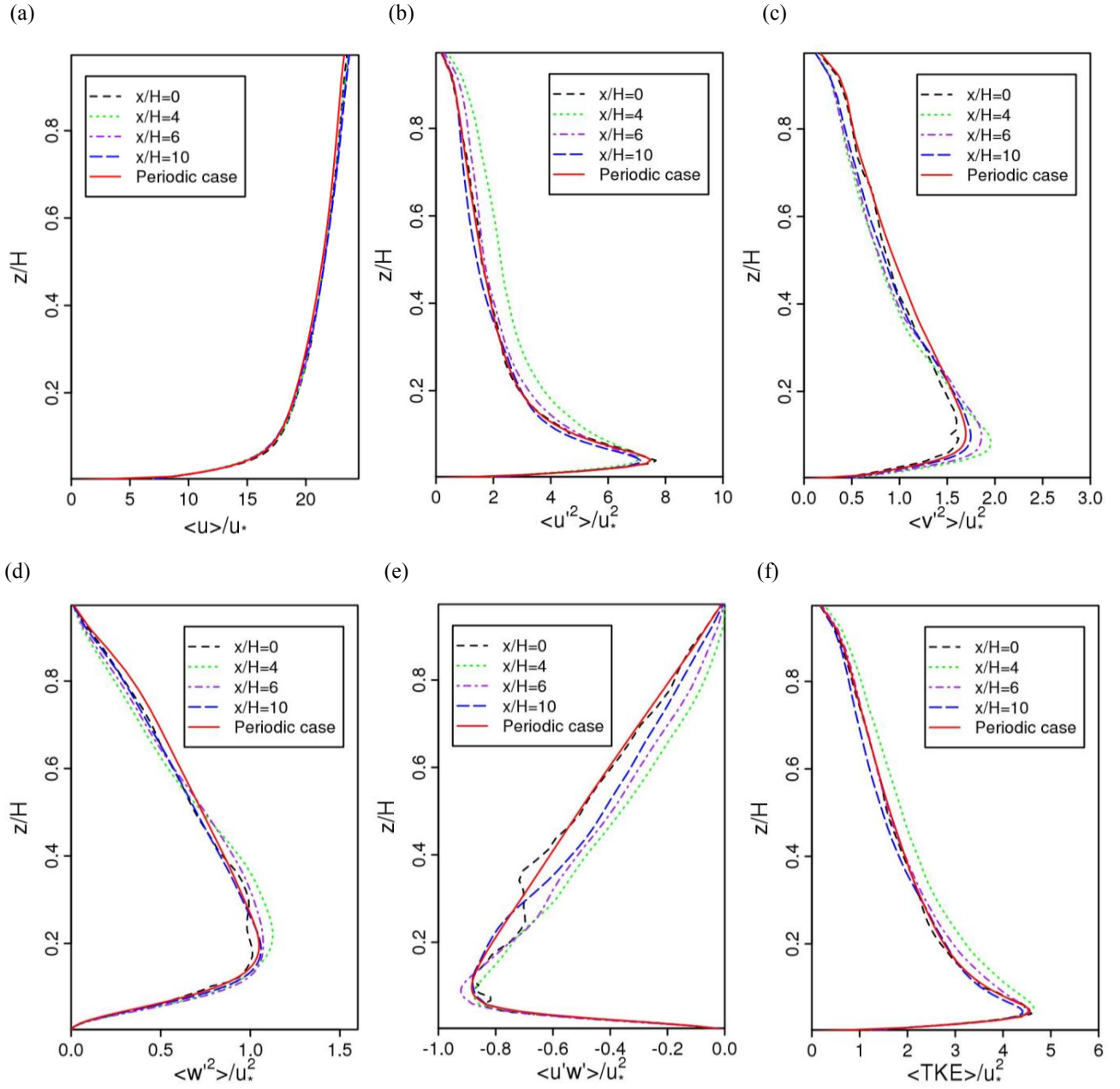


Figure 4: Horizontal profiles (spatially and temporally averaged) of (a) $\langle u \rangle / u_*$, (b) $\langle u'^2 \rangle / u_*^2$, (c) $\langle v'^2 \rangle / u_*^2$, (d) $\langle w'^2 \rangle / u_*^2$, (e) $\langle u'w' \rangle / u_*^2$, and (f) $\langle TKE \rangle / u_*^2$ at $z/H=0.1$ and $z/H=0.5$ in the periodic case and the inflow case (LS1.0).



5 Figure 5: Spatially and temporally averaged vertical profiles of (a) $\langle u \rangle / u_*$, (b) $\langle u'^2 \rangle / u_*^2$, (c) $\langle v'^2 \rangle / u_*^2$, (d) $\langle w'^2 \rangle / u_*^2$, (e) $\langle u'w' \rangle / u_*^2$, and (f) $\langle TKE \rangle / u_*^2$ at a series of downwind locations in the inflow case (LS1.0), and the periodic case (also averaged in the streamwise direction).

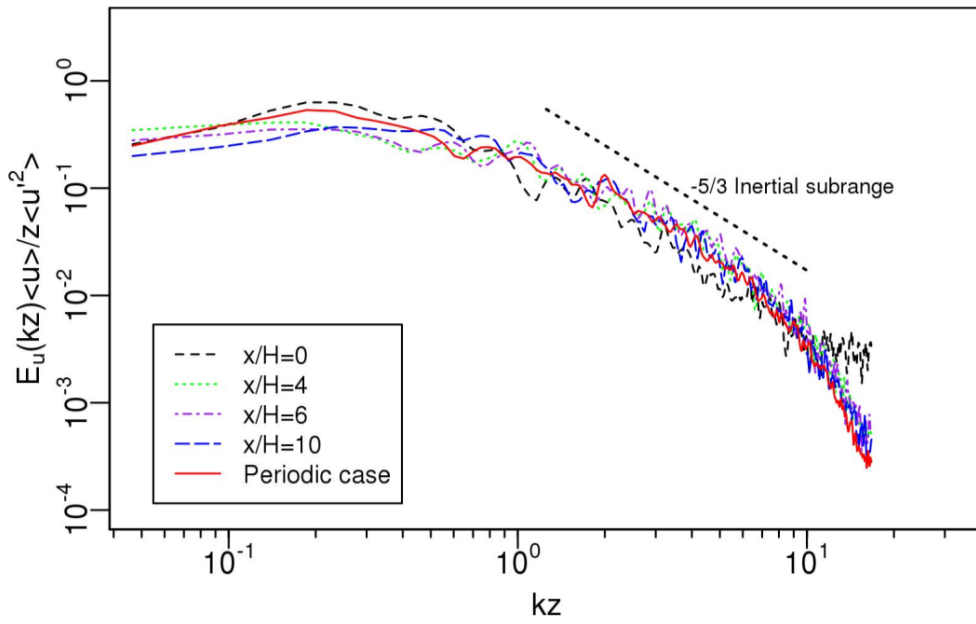


Figure 6: Spectra of streamwise wind component for a series of downwind locations at the height of $z/H=0.5$, k is the angular wavenumber, with $\langle \mathbf{u} \rangle$ and $\langle \mathbf{u}'^2 \rangle$ the **spatially** averaged mean and streamwise normal Reynolds stress, respectively.

5

10

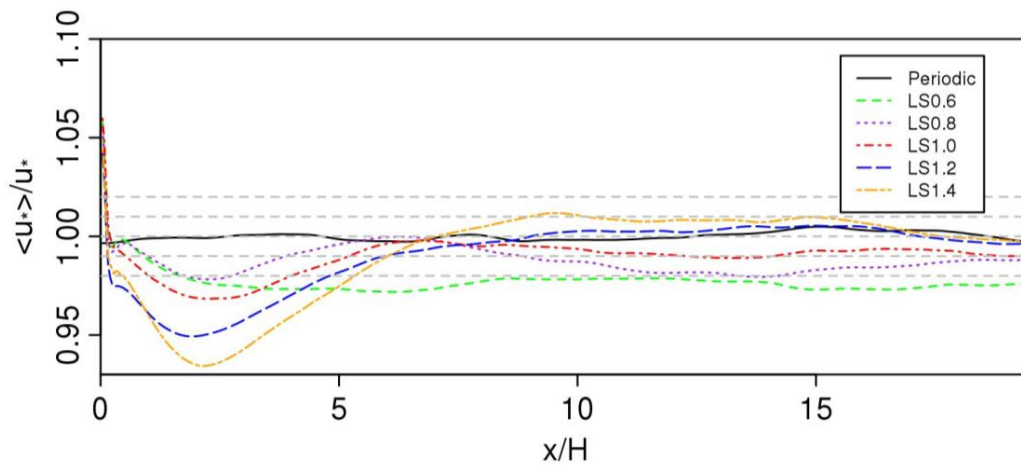


Figure 7: Development of local friction velocity (averaged over spanwise direction and time) with various integral length scales. $\langle u_* \rangle$ is the local friction velocity along the streamwise direction, and u_*^* is the x-y-t-averaged friction velocity for the periodic case.

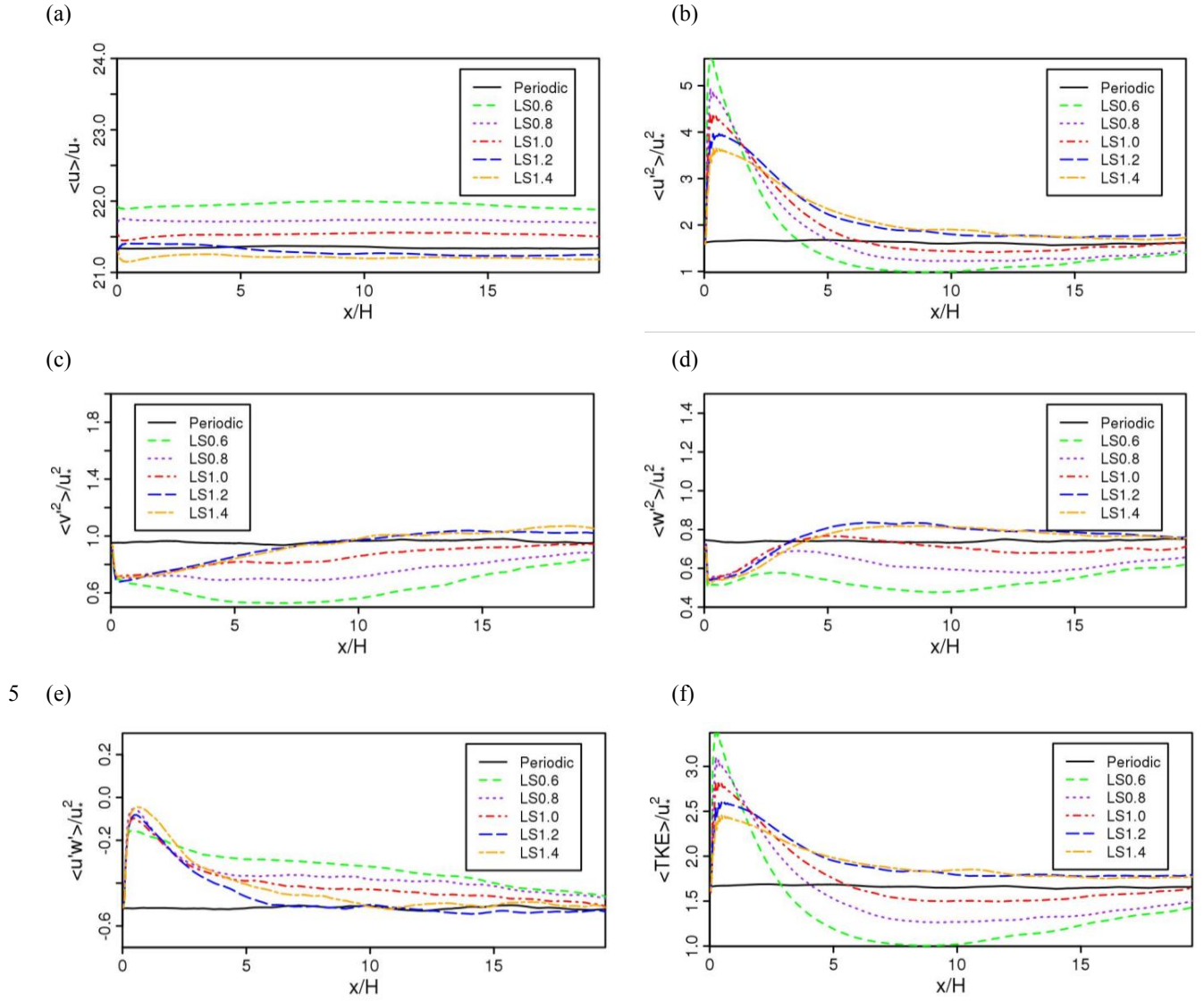
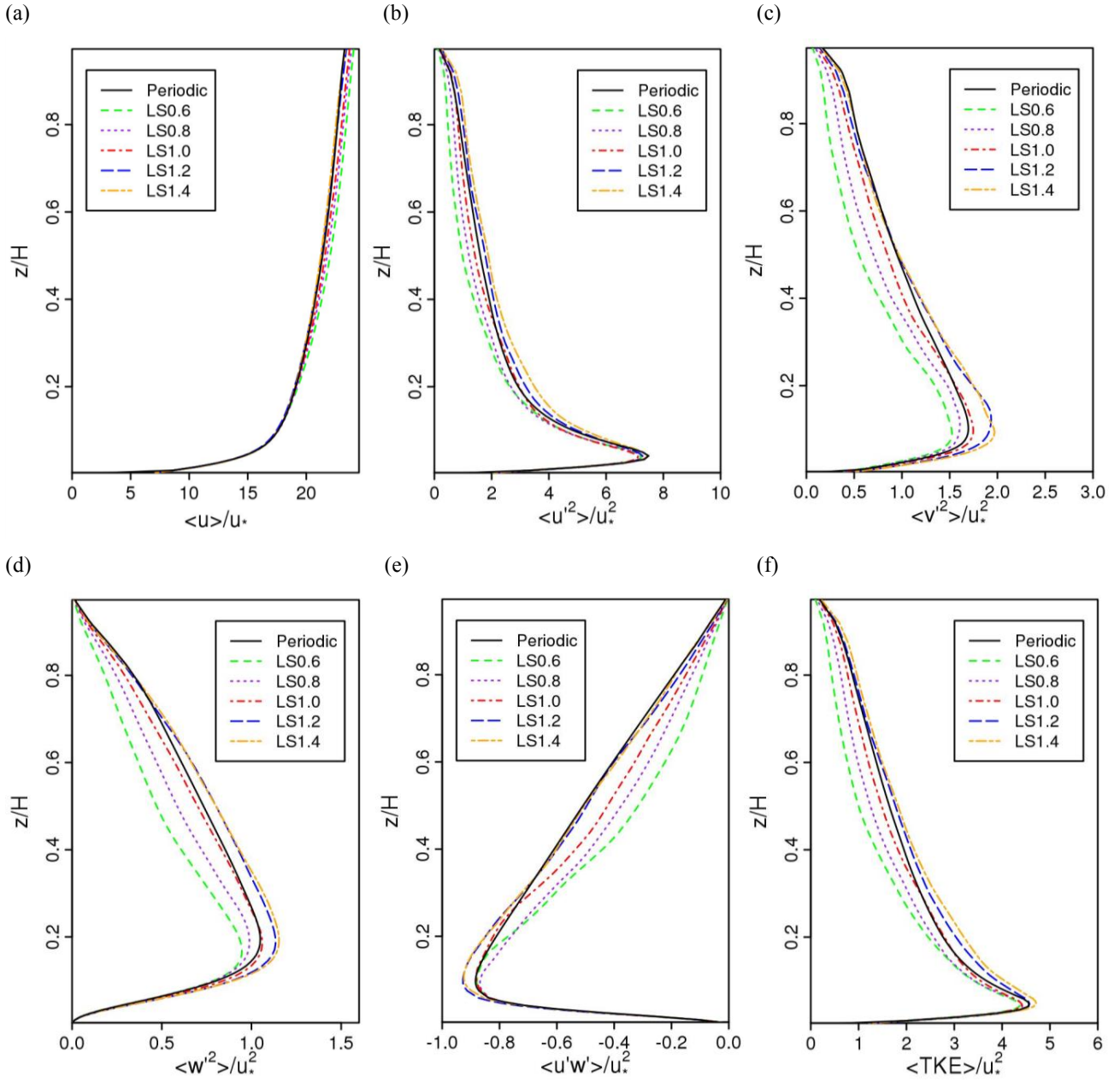


Figure 8: Horizontal profiles (spatially and temporally averaged) of (a) $\langle u \rangle / u_*$, (b) $\langle u'^2 \rangle / u_*^2$, (c) $\langle v'^2 \rangle / u_*^2$, (d) $\langle w'^2 \rangle / u_*^2$, (e) $\langle u'w' \rangle / u_*^2$, and (f) $\langle TKE \rangle / u_*^2$ at $z/H=0.5$ with various integral length scales.



5 Figure 9: Vertical profiles (spatially and temporally averaged) of (a) $\langle u \rangle / u_*$, (b) $\langle u'^2 \rangle / u_*^2$, (c) $\langle v'^2 \rangle / u_*^2$, (d) $\langle w'^2 \rangle / u_*^2$, (e) $\langle u'w' \rangle / u_*^2$, and (f) $\langle TKE \rangle / u_*^2$ at $x/H=10$ with various integral length scales.

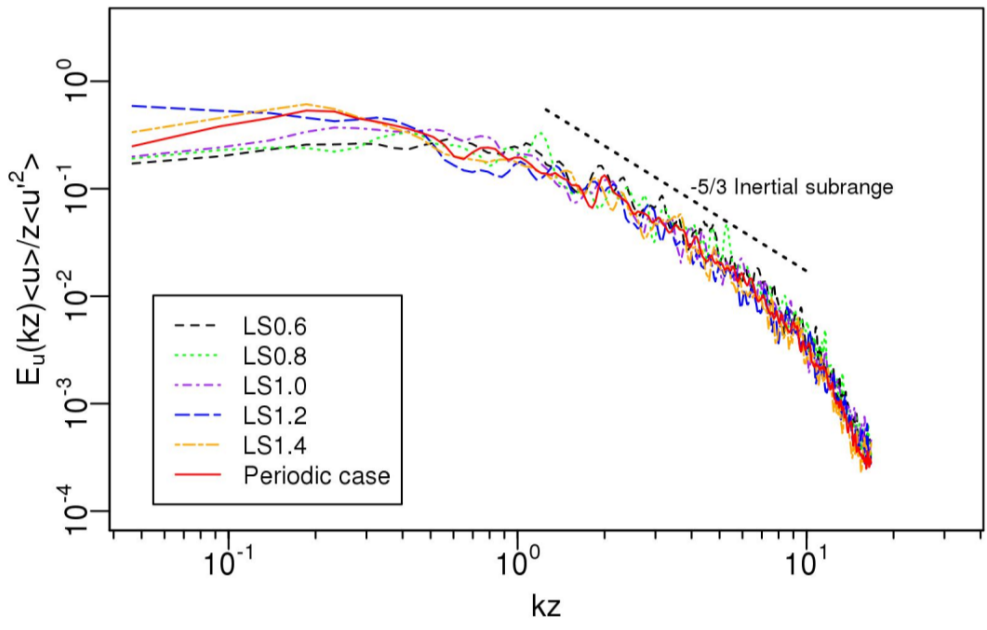


Figure 10: Spectra of streamwise wind component for a series of downwind locations at $x/H=10$ and $z/H=0.5$ with various integral length scales, k is the angular wavenumber, with $\langle u \rangle$ and $\langle u'^2 \rangle$ the spatially averaged mean and streamwise normal Reynolds stress, respectively.

5

10

15

References

- Benhamadouche, S., Jarrin, N., Addad, Y., and Laurence, D.: Synthetic turbulent inflow conditions based on a vortex method for large-eddy simulation, *Progress in Computational Fluid Dynamics*, 6, 50-57, 10.1504/pcfd.2006.009482, 2006.
- 5 Bercin, K. M., Xie, Z. T., and Turnock, S. R.: Exploration of digital-filter and forward-stepwise synthetic turbulence generators and an improvement for their skewness-kurtosis, *Computers & Fluids*, 172, 443-466, 10.1016/j.compfluid.2018.03.070, 2018.
- Berkooz, G., Holmes, P., and Lumley, J. L.: The proper orthogonal decomposition in the analysis of turbulent flows, *Annual Review of Fluid Mechanics*, 25, 539-575, 10.1146/annurev.fl.25.010193.002543, 1993.
- 10 Chu, X., Xue, L. L., Geerts, B., Rasmussen, R., and Breed, D.: A Case Study of Radar Observations and WRF LES Simulations of the Impact of Ground-Based Glaciogenic Seeding on Orographic Clouds and Precipitation. Part I: Observations and Model Validations, *Journal of Applied Meteorology and Climatology*, 53, 2264-2286, 10.1175/jamc-d-14-0017.1, 2014.
- Deardorff, J. W.: A numerical study of three-dimensional turbulent channel flow at large Reynolds numbers, *Journal of Fluid Mechanics*, 41, 453-480, 10.1017/s0022112070000691, 1970.
- 15 Dhamankar, N. S., Blaisdell, G. A., and Lyrintzis, A. S.: Overview of Turbulent Inflow Boundary Conditions for Large-Eddy Simulations, *Aiaa Journal*, 56, 1317-1334, 10.2514/1.j055528, 2018.
- Doubrawa, P., Montornès, A., Barthelmie, R. J., Pryor, S. C., and Casso, P.: Analysis of Different Gray Zone Treatments in WRF-LES Real Case Simulations, *Wind Energ. Sci. Discuss.*, <https://doi.org/10.5194/wes-2017-5161>, 2018, 10.1146/annurev.fluid.35.101101.161147, 2018.
- 20 Ghannam, K., Poggi, D., Porporato, A., and Katul, G. G.: The Spatio-temporal Statistical Structure and Ergodic Behaviour of Scalar Turbulence Within a Rod Canopy, *Boundary-Layer Meteorology*, 157, 447-460, 10.1007/s10546-015-0073-1, 2015.
- Jarrin, N., Benhamadouche, S., Laurence, D., and Prosser, R.: A synthetic-eddy-method for generating inflow conditions for large-eddy simulations, *International Journal of Heat and Fluid Flow*, 27, 585-593, 10.1016/j.ijheatfluidflow.2006.02.006, 25 2006.
- Kang, S. L., and Lenschow, D. H.: Temporal Evolution of Low-Level Winds Induced by Two-dimensional Mesoscale Surface Heat-Flux Heterogeneity, *Boundary-Layer Meteorology*, 151, 501-529, 10.1007/s10546-014-9912-8, 2014.
- Keating, A., Piomelli, U., Balaras, E., and Kaltenbach, H. J.: A priori and a posteriori tests of inflow conditions for large-eddy simulation, *Physics of Fluids*, 16, 4696-4712, 10.1063/1.1811672, 2004.
- 30 Kempf, A., Klein, M., and Janicka, J.: Efficient generation of initial- and inflow-conditions for transient turbulent flows in arbitrary geometries, *Flow Turbulence and Combustion*, 74, 67-84, 10.1007/s10494-005-3140-8, 2005.
- Kerschen, G., Golinval, J. C., Vakakis, A. F., and Bergman, L. A.: The method of proper orthogonal decomposition for dynamical characterization and order reduction of mechanical systems: An overview, *Nonlinear Dynamics*, 41, 147-169, 10.1007/s11071-005-2803-2, 2005.
- 35 Khani, S., and Porte-Agel, F.: A Modulated-Gradient Parametrization for the Large-Eddy Simulation of the Atmospheric Boundary Layer Using the Weather Research and Forecasting Model, *Boundary-Layer Meteorology*, 165, 385-404, 10.1007/s10546-017-0287-5, 2017.
- Kim, Y., Castro, I. P., and Xie, Z. T.: Divergence-free turbulence inflow conditions for large-eddy simulations with incompressible flow solvers, *Computers & Fluids*, 84, 56-68, 10.1016/j.compfluid.2013.06.001, 2013.
- 40 Kim, Y., and Xie, Z. T.: Modelling the effect of freestream turbulence on dynamic stall of wind turbine blades, *Computers & Fluids*, 129, 53-66, 10.1016/j.compfluid.2016.02.004, 2016.
- Kirkil, G., Mirocha, J., Bou-Zeid, E., Chow, F. K., and Kosovic, B.: Implementation and Evaluation of Dynamic Subfilter-Scale Stress Models for Large-Eddy Simulation Using WRF, *Monthly Weather Review*, 140, 266-284, 10.1175/mwr-d-11-00037.1, 2012.
- 45 Klein, M., Sadiki, A., and Janicka, J.: A digital filter based generation of inflow data for spatially developing direct numerical or large eddy simulations, *Journal of Computational Physics*, 186, 652-665, 10.1016/s0021-9991(03)00090-1, 2003.
- Kraichnan, R. H.: Diffusion by a Random Velocity Field, *Physics of Fluids*, 13, 22-31, 10.1063/1.1692799, 1970.

- Laraufie, R., Deck, S., and Sagaut, P.: A dynamic forcing method for unsteady turbulent inflow conditions, *Journal of Computational Physics*, 230, 8647-8663, 10.1016/j.jcp.2011.08.012, 2011.
- Lee, S., Lele, S. K., and Moin, P.: Simulation of spatially evolving turbulence and the applicability of Taylor's hypothesis in compressible flow, *Physics of Fluids A-Fluid Dynamics*, 4, 1521-1530, 10.1063/1.858425, 1992.
- 5 Liu, Y. B., Warner, T., Liu, Y. W., Vincent, C., Wu, W. L., Mahoney, B., Swerdlin, S., Parks, K., and Boehnert, J.: Simultaneous nested modeling from the synoptic scale to the LES scale for wind energy applications, *Journal of Wind Engineering and Industrial Aerodynamics*, 99, 308-319, 10.1016/j.jweia.2011.01.013, 2011.
- Lund, T. S., Wu, X. H., and Squires, K. D.: Generation of turbulent inflow data for spatially-developing boundary layer simulations, *Journal of Computational Physics*, 140, 233-258, 10.1006/jcph.1998.5882, 1998.
- 10 Ma, Y. L., and Liu, H. P.: Large-Eddy Simulations of Atmospheric Flows Over Complex Terrain Using the Immersed-Boundary Method in the Weather Research and Forecasting Model, *Boundary-Layer Meteorology*, 165, 421-445, 10.1007/s10546-017-0283-9, 2017.
- Maronga, B., Banzhaf, S., Burmeister, C., Esch, T., Forkel, R., Fröhlich, D., Fuka, V., Gehrke, K. F., Geletič, J., Giersch, S., Gronemeier, T., Groß, G., Heldens, W., Hellsten, A., Hoffmann, F., Inagaki, A., Kadasch, E., Kanani-Sühring, F., Ketelsen, 15 K., Khan, B. A., Knigge, C., Knoop, H., Krč, P., Kurppa, M., Maamari, H., Matzarakis, A., Mauder, M., Pallasch, M., Pavlik, D., Pfafferoth, J., Resler, J., Rissmann, S., Russo, E., Salim, M., Schrempf, M., Schwenkel, J., Seckmeyer, G., Schubert, S., Sühring, M., von Tils, R., Vollmer, L., Ward, S., Witha, B., Wurps, H., Zeidler, J., and Raasch, S.: Overview of the PALM model system 6.0, *Geosci. Model Dev. Discuss.*, 2019, 1-63, 10.5194/gmd-2019-103, 2019.
- Mazzaro, L. J., Koo, E., Munoz-Esparza, D., Lundquist, J. K., and Linn, R. R.: Random Force Perturbations: A New 20 Extension of the Cell Perturbation Method for Turbulence Generation in Multiscale Atmospheric Boundary Layer Simulations, *Journal of Advances in Modeling Earth Systems*, 11, 2311-2329, 10.1029/2019ms001608, 2019.
- Mirocha, J., Kosovic, B., and Kirkil, G.: Resolved Turbulence Characteristics in Large-Eddy Simulations Nested within Mesoscale Simulations Using the Weather Research and Forecasting Model, *Monthly Weather Review*, 142, 806-831, 10.1175/mwr-d-13-00064.1, 2014.
- 25 Moeng, C. H., Dudhia, J., Klemp, J., and Sullivan, P.: Examining two-way grid nesting for large eddy simulation of the PBL using the WRF model, *Monthly Weather Review*, 135, 2295-2311, 10.1175/mwr3406.1, 2007.
- Morgan, B., Larsson, J., Kawai, S., and Lele, S. K.: Improving Low-Frequency Characteristics of Recycling/Rescaling Inflow Turbulence Generation, *Aiaa Journal*, 49, 582-597, 10.2514/1.j050705, 2011.
- Munoz-Esparza, D., Kosovic, B., Mirocha, J., and van Beeck, J.: Bridging the Transition from Mesoscale to Microscale 30 Turbulence in Numerical Weather Prediction Models, *Boundary-Layer Meteorology*, 153, 409-440, 10.1007/s10546-014-9956-9, 2014.
- Munoz-Esparza, D., Kosovic, B., van Beeck, J., and Mirocha, J.: A stochastic perturbation method to generate inflow turbulence in large-eddy simulation models: Application to neutrally stratified atmospheric boundary layers, *Physics of Fluids*, 27, 10.1063/1.4913572, 2015.
- 35 Munoz-Esparza, D., and Kosovic, B.: Generation of Inflow Turbulence in Large-Eddy Simulations of Nonneutral Atmospheric Boundary Layers with the Cell Perturbation Method, *Monthly Weather Review*, 146, 1889-1909, 10.1175/mwr-d-18-0077.1, 2018.
- Munters, W., Meneveau, C., and Meyers, J.: Turbulent Inflow Precursor Method with Time-Varying Direction for Large-Eddy Simulations and Applications to Wind Farms, *Boundary-Layer Meteorology*, 159, 305-328, 10.1007/s10546-016- 40 0127-z, 2016.
- Nottrott, A., Kleissl, J., and Keeling, R.: Modeling passive scalar dispersion in the atmospheric boundary layer with WRF large-eddy simulation, *Atmospheric Environment*, 82, 172-182, 10.1016/j.atmosenv.2013.10.026, 2014.
- Nunalee, C. G., Kosovic, B., and Bieringer, P. E.: Eulerian dispersion modeling with WRF-LES of plume impingement in neutrally and stably stratified turbulent boundary layers, *Atmospheric Environment*, 99, 571-581, 45 10.1016/j.atmosenv.2014.09.070, 2014.
- PALM, <https://palm.muk.uni-hannover.de/trac/changeset/2259>, 10.1016/j.compfluid.2014.11.005, 2017.
- Schluter, J. U., Pitsch, H., and Moin, P.: Large eddy simulation inflow conditions for coupling with Reynolds-averaged flow solvers, *Aiaa Journal*, 42, 478-484, 10.2514/1.3488, 2004.
- Skamarock, W. C., and Klemp, J. B.: A time-split nonhydrostatic atmospheric model for weather research and forecasting 50 applications, *Journal of Computational Physics*, 227, 3465-3485, 10.1016/j.jcp.2007.01.037, 2008.

- Tabor, G. R., and Baba-Ahmadi, M. H.: Inlet conditions for large eddy simulation: A review, *Computers & Fluids*, 39, 553-567, 10.1016/j.compfluid.2009.10.007, 2010.
- Talbot, C., Bou-Zeid, E., and Smith, J.: Nested Mesoscale Large-Eddy Simulations with WRF: Performance in Real Test Cases, *Journal of Hydrometeorology*, 13, 1421-1441, 10.1175/jhm-d-11-048.1, 2012.
- 5 Veloudis, I., Yang, Z., McGuirk, J. J., Page, G. J., and Spencer, A.: Novel implementation and assessment of a digital filter based approach for the generation of LES inlet conditions, *Flow Turbulence and Combustion*, 79, 1-24, 10.1007/s10494-006-9058-y, 2007.
- Wu, X. H.: Inflow Turbulence Generation Methods, in: *Annual Review of Fluid Mechanics*, Vol 49, edited by: Davis, S. H., and Moin, P., *Annual Review of Fluid Mechanics*, 23-49, 2017.
- 10 Xie, Z. T., and Castro, I. P.: Efficient generation of inflow conditions for large eddy simulation of street-scale flows, *Flow Turbulence and Combustion*, 81, 449-470, 10.1007/s10494-008-9151-5, 2008.
- Xie, Z. T., and Castro, I. P.: Large-eddy simulation for flow and dispersion in urban streets, *Atmospheric Environment*, 43, 2174-2185, 10.1016/j.atmosenv.2009.01.016, 2009.
- 15 Zhu, X. L., Ni, G. H., Cong, Z. T., Sun, T., and Li, D.: Impacts of surface heterogeneity on dry planetary boundary layers in an urban-rural setting, *Journal of Geophysical Research-Atmospheres*, 121, 12164-12179, 10.1002/2016jd024982, 2016.